

# Nuclear Energy Density Functionals: What do we really know?

Aurel Bulgac,<sup>1,\*</sup> Michael McNeil Forbes,<sup>2,1,†</sup> and Shi Jin<sup>1,‡</sup>

<sup>1</sup>*Department of Physics,  
University of Washington, Seattle,  
Washington 98195–1560,  
USA*

<sup>2</sup>*Department of Physics & Astronomy,  
Washington State University,  
Pullman, Washington 99164–2814,  
USA*

(Dated: July 1, 2015)

We present the simplest nuclear energy density functional (NEDF) to date, determined by only 4 significant phenomenological parameters, yet capable of fitting measured nuclear masses with better accuracy than the Bethe-Weizsäcker mass formula, while also describing density structures (charge radii, neutron skins etc.) and time-dependent phenomena (induced fission, giant resonances, low energy nuclear collisions, etc.). The 4 significant parameters are necessary to describe bulk nuclear properties (binding energies and charge radii); an additional 2 to 3 parameters have little influence on the bulk nuclear properties, but allow independent control of the density dependence of the symmetry energy, excitation energy of isovector excitations, and the Thomas-Reiche-Kuhn sum rule. This Hohenberg-Kohn-style of density functional theory (DFT) successfully realizes Weizsäcker's ideas and provides a computationally tractable model for a variety of static nuclear properties and dynamics, from finite nuclei to neutron stars, where it will also provide a new insight into the physics of the r-process, nucleosynthesis, neutron star crust structure, and neutron star mergers. This new NEDF clearly separates the bulk geometric properties – volume, surface, symmetry, and Coulomb energies which amount to  $\sim 8$  MeV per nucleon or up to  $\sim 2000$  MeV per nucleus for heavy nuclei – from finer details related to shell effects, pairing, isospin breaking, etc. which contribute at most a few MeV for the entire nucleus. Thus it provides a systematic framework for organizing various contributions to the NEDF. Measured and calculated physical observables – i.e. symmetry and saturation properties, the neutron matter equation of state, and the frequency of giant dipole resonances – lead directly to new terms, not considered in current NEDF parameterizations.

## CONTENTS

I. Introduction	1	VI. Supplemental material	21
II. Static Properties	4	References	21
A. Form of the NEDF	5		
B. Gradient Terms	6		
C. Infinite Nuclear and Neutron Matter	7		
III. Fitting Masses and Charge Radii	8		
A. Discussion	9		
B. Neutron Matter	10		
C. Saturation and Symmetry Properties	11		
D. Symmetry Energy and Neutron Skin Thickness	12		
E. Neutron Drip Line	12		
F. Charge Radii	13		
G. Principal Component Analysis	15		
IV. Dynamical Properties	16		
A. Entrainment	17		
B. Shell Effects	18		
C. Induced Symmetric and Asymmetric Fission	19		
D. Giant Isovector Resonances	19		
V. Conclusions	20		
Acknowledgments	21		

## I. INTRODUCTION

Calculating nuclear masses, nuclear matter and charge distributions, and dynamics in nuclear systems remains one of the most challenging problems in quantum many-body theory. Almost a century ago, Aston (1920) realized that a nucleus is not quite the sum of its parts, leading Eddington (1920) to correctly conjecture a link between nuclear masses, the conversion of hydrogen into heavier elements, and the energy radiated by the stars. When quantum mechanics was first applied to many-body systems, Weizsäcker (1935) proposed that an energy density approach could be effective for calculating nuclear binding energies. This was the first instance of an energy density functional being applied in nuclear physics, with the fundamentals of DFT laid several decades later (Dreizler and Gross, 1990; Hohenberg and Kohn, 1964; Kohn and Sham, 1965). Bethe and Bacher (1936) further developed Weizsäcker's ideas and introduced the nuclear mass formula (known as the Bethe-Weizsäcker formula) for the ground state energies of nuclei with  $A = N + Z$  nucleons ( $N$  neutrons and  $Z$

\* bulgac@uw.edu

† mforbes@alum.mit.edu

‡ kingstone1991@gmail.com

$a_v$	$a_s$	$a_I$	$a'_I$	$a_C$	$a'_C$	$\delta$	$\chi_E$
-15.46	16.71	22.84	0	0.698	0	0	3.30
-15.48	16.76	22.88	0	0.699	0	12.29	3.17
-15.31	17.74	24.94	-22.50	0.765	-0.667	0	2.64
-15.34	17.78	24.99	-22.33	0.765	-0.653	11.46	2.50

Table I Parameters and the energy rms of the mass formulas Eqs. (1) or (2), with or without the contribution Eq. (2b) for 2375 nuclei from Audi *et al.* (2012) and Wang *et al.* (2012). (All quantities express in MeV.)

protons):

$$E(N, Z) = a_v A + a_s A^{2/3} + a_C \frac{Z^2}{A^{1/3}} + a_I \frac{(N-Z)^2}{A}. \quad (1)$$

Unlike electrons in atoms, nuclei are saturating systems with a nearly constant interior density, yielding the terms above: a volume energy, a surface tension, a non-extensive Coulomb energy, and a symmetry energy that favors similar numbers of protons and neutrons. As shown in the first row of Table I, these four terms alone fit the latest evaluated nuclear masses (Audi *et al.*, 2012; Wang *et al.*, 2012) with a root-mean-square (rms) error of  $\chi_E \approx 3$  MeV per nucleus, where  $\chi_E^2 = \sum |E_{N,Z} - E(N, Z)|^2 / N_E$  and we fit the  $N_E = 2375$  measured (not extrapolated) nuclear masses of nuclei with  $A \geq 16$  from Audi *et al.* (2012) and Wang *et al.* (2012). This is a remarkable result: the nuclear binding energy of heavy nuclei can reach 2000 MeV, hence the errors are at the sub-percent level.

A slightly better fit is obtained using a mass formula with surface corrections terms to the symmetry and Coulomb energies, as well as odd-even staggering (due to pairing):

$$E(N, Z) = a_v A + a_s A^{2/3} + a_C \frac{Z^2}{A^{1/3}} + a'_C \frac{Z^2}{A^{2/3}} + a_I \frac{(N-Z)^2}{A} + a'_I \frac{(N-Z)^2}{A^{4/3}} + \Delta. \quad (2a)$$

$$\Delta = \begin{cases} -\delta A^{-1/2} & \text{even-even nuclei,} \\ 0 & \text{odd nuclei,} \\ \delta A^{-1/2} & \text{odd-odd nuclei.} \end{cases} \quad (2b)$$

This pairing contribution is significantly smaller than the others, with an amplitude  $\approx 12 \text{ MeV} / A^{1/2}$ ; it is also smaller than contributions arising from shell-correction energies, changing the rms error  $\chi_E$  by about at most 100 keV to 150 keV. The results of this fit are shown in Table I with the overall residuals displayed in Fig. 1. The magnitudes of the various terms are compared in Fig. 2. While the volume, surface, and Coulomb contributions are clearly dominant to the nuclear binding energy, the symmetry energy contributions are roughly at the level of 10% at most.

In parallel, a number of properties of many-fermion systems were understood mathematically by tying together the roles of

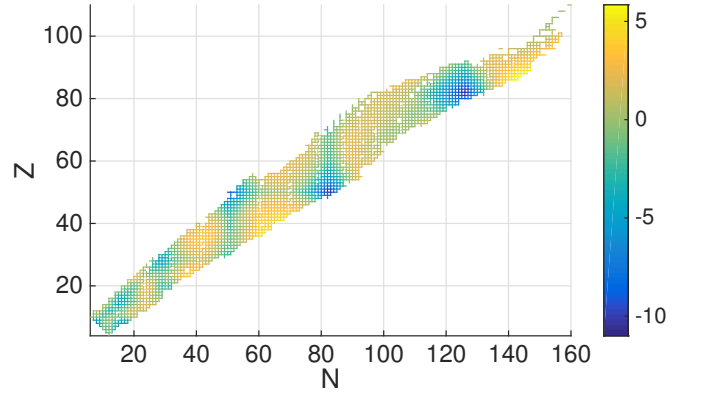


Figure 1 (Color online) The differences  $E_{\text{exp}} - E_{\text{th}}$  in MeVs between the evaluated ground state energies (Audi *et al.*, 2012; Wang *et al.*, 2012) of 2375 nuclei with  $A \geq 16$  and fitted with the 6-parameter mass formula Eq. (2) and  $\Delta \equiv 0$ . One can easily identify the emergence of closed shells for protons and neutrons.

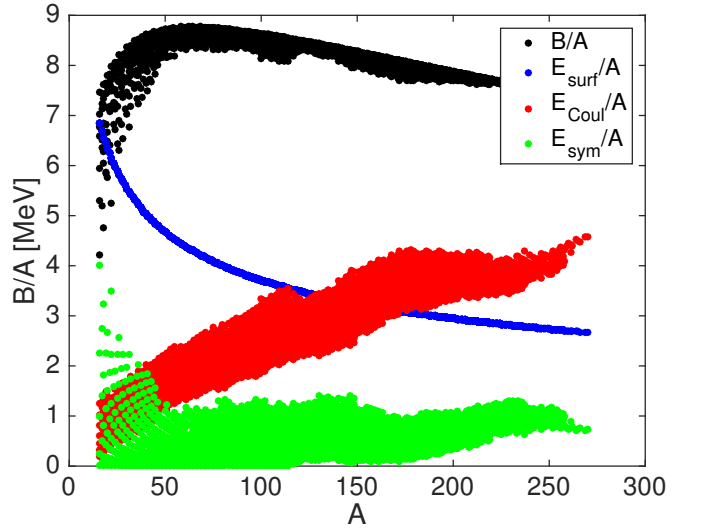


Figure 2 (Color online) The binding energy per nucleon  $B/A = |E(N, Z)|/A$  and the Coulomb, surface and symmetry energy per nucleon in Eq. (2) for the measured 2375 nuclei with  $A \geq 16$  (Audi *et al.*, 2012; Wang *et al.*, 2012).

the geometry and of the periodic trajectories in cavities. As early as 1911, Weyl (1911, 1912a,b,c, 1913, 1915, 1950) and others related the wave eigenstate density in boxes of various shapes and boundary conditions to the geometrical shape of the box (Baltes and Hilf, 1976; Brack and Bhaduri, 1997; Kac, 1966; Waechter, 1972). In a manner very similar to the nuclear mass formula Eq. (1), such formulas can be applied to saturating systems, relating the ground state energy to the volume ( $V$ ), surface area ( $A$ ), and mean curvature radius  $R$  of the many-particle system:

$$E = a_v V + a_s S + a_R R + \dots \quad (3)$$

The similarity to the nuclear mass formula Eq. (1) becomes apparent after relating the volume to the particle number  $\rho = A/V \approx \text{const.}$  (The Coulomb repulsion energy should be

evaluated separately in a straightforward manner, due to the long-range character of the interaction.) The ground state energy can thus be rewritten in terms of particle number  $A$  (here for only one kind of particles)

$$E = b_V A + b_S A^{2/3} + b_R A^{1/3} + \dots \quad (4)$$

The coefficient  $b_V$  is the energy per particle in infinite matter and  $a_S$  represents the surface tension. These types of expansion are essentially classical in character, with Planck's constant playing no explicit role, and their accuracy for many-fermion system is limited by the lack of quantum effects (referred often as shell effects). It appears that for nuclei the mass formula Eq. (2) is about as good as one can achieve without introducing the quantum effects.

Balian and Bloch (1970, 1971, 1972) observed that quantum states in a finite system can be quite accurately reproduced by quantizing the periodic classical trajectories. Combining the idea of geometrical quantization with the Thomas-Fermi model, the Pauli principle, and copious empirical evidence that strongly interacting fermionic systems share many similarities with non-interacting systems (Haxel *et al.*, 1949; Landau, 1956, 1957; Mayer, 1949, 1950a,b; Migdal, 1967), one can quite accurately construct the single-particle density of states and binding energies as a function of the particle number, eventually correcting this by the shape of the system.

The single-particle density of states  $\rho(\varepsilon)$  in a given potential has a smooth and an oscillating components:

$$\rho(\varepsilon) = \rho_{\text{TF}}(\varepsilon) + \rho_{\text{osc}}(\varepsilon), \quad (5a)$$

$$\rho_{\text{osc}}(\varepsilon) = \sum_{\text{PO}} a_{\text{PO}}(\varepsilon) \sin\left(\frac{S_{\text{PO}}(\varepsilon)}{\hbar} + \phi_{\text{PO}}\right) + \dots, \quad (5b)$$

where the sum is performed over classical periodic orbits (PO) (diameter, triangles, squares, etc.),  $a_{\text{PO}}(\varepsilon)$  is the stability amplitude,  $S_{\text{PO}}(\varepsilon)$  the action, and  $\phi_{\text{PO}}$  the Maslov index of each orbit at the energy  $\varepsilon$  (Balian and Bloch, 1970, 1971, 1972; Brack and Bhaduri, 1997; Nishioka *et al.*, 1990). The single-particle density of states in the Thomas-Fermi approximation  $\rho_{\text{TF}}$  (Baltes and Hilf, 1976; Brack and Bhaduri, 1997; Kac, 1966; Waechter, 1972; Weyl, 1911, 1912a,b,c, 1913, 1915, 1950) has a clear dependence on the size and shape of the system, and leads to Eqs. (3) and (4) for a square-well potential. At the same time, the nature of the periodic orbits also depends on the size and shape of the single-particle potential.

Knowing  $\rho(\varepsilon)$ , one can calculate the particle number  $A$  and shell-corrections (SC) energy  $E_{\text{SC}} = E - E_{\text{TF}}$  for a many-fermion system by integrating up to the chemical potential  $\mu$ :

$$A = \int_{-\infty}^{\mu} \rho(\varepsilon) d\varepsilon, \quad E_{\text{SC}} = \int_{-\infty}^{\mu} \varepsilon \rho_{\text{osc}}(\varepsilon) d\varepsilon. \quad (6)$$

The theory of periodic orbits and structure of these shell-corrections has been studied extensively. For example, in a 3-dimensional spherical cavity, quantum effects can be reproduced by including only triangular and square orbits (Balian

and Bloch, 1970, 1971, 1972; Brack and Bhaduri, 1997; Nishioka *et al.*, 1990). The emergence of magic numbers, and the role of the shapes of many-fermion systems have been tested in theory and validated against experimental results in fermion systems with up to 3000 electrons (Brack, 1993; de Heer, 1993; Pedersen *et al.*, 1991). In particular, in atomic clusters the emergence of the super-shells has been predicted theoretically (Brack, 1993; Bulgac and Lewenkopf, 1993; Nishioka *et al.*, 1990) and confirmed experimentally (de Heer, 1993; Pedersen *et al.*, 1991), though nuclei are too small to exhibit the emergence of super-shells.

In nuclear physics a similar line of inquiry is encapsulated in the method of shell-corrections, developed by Strutinsky (Strutinsky, 1966, 1967, 1968) and others (Bohr and Mottelson, 1998; Brack *et al.*, 1972, 1985; Moller *et al.*, 1995; Möller *et al.*, 2012; Myers and Swiatecki, 1974, 1990, 1991, 1996, 1969, 1966; Ring and Schuck, 2004; Strutinsky and Magner, 1976), which shows that  $\rho(\varepsilon)$  has a well defined dependence on the particle number. The smooth part of the density of states is well described by the Thomas-Fermi approximation (and alternatively by the smoothing procedure introduced by Strutinsky), the leading terms of which are the volume ( $\sim A$ ), surface ( $\sim A^{2/3}$ ), Coulomb ( $\sim Z^2/A^{1/3}$ ), and symmetry energy ( $\sim (N-Z)^2/A$ ) contributions encoded in the Bethe-Weizsäcker mass formula (1). The oscillating part is dominated by the nuclear shape and the shell effects from the periodic orbits, with an amplitude dependent on the particle number as  $A^{1/6}$  (Strutinsky and Magner, 1976).

This separation of  $\rho(\varepsilon)$  into the smooth and oscillating parts (5a) is a general characteristic of the many fermion systems. Both the macroscopic-microscopic method (Bohr and Mottelson, 1998; Brack *et al.*, 1972, 1985; Moller *et al.*, 1995; Möller *et al.*, 2012; Myers and Swiatecki, 1974, 1990, 1991, 1996, 1969, 1966; Ring and Schuck, 2004; Strutinsky, 1966, 1967, 1968; Strutinsky and Magner, 1976) and self-consistent approaches (Bender *et al.*, 2003; Delaroche *et al.*, 2010; Goriely and Capote, 2014; Goriely *et al.*, 2009, 2013; Kotrelainen *et al.*, 2014b) lead to the same conclusions about the various contributions described above, and agree with experimental data (Lunney *et al.*, 2003). This suggests the question: To what order can one expand the density of states in powers of the particle numbers and periodic orbits?

There is a reasonable consensus that, beyond the leading contributions from the periodic orbits and shell-corrections, such an expansion fails due to the effects of quantum chaos – i.e. contributions from classically chaotic trajectories through the many-body phase space (Bohigas *et al.*, 1993). Stable periodic orbits provide the strongest shell effects in quantum systems, evident for example in the magic numbers (see e.g. Fig. 4). Unstable periodic orbits also produce shell effects, but typically with smaller weights. In contrast, chaotic orbits appear to produce irregular oscillations in the single-particle density of states with a rather small amplitude. Various estimates suggest that chaotic fluctuations appear at the level of 0.5 MeV per nucleus (Åberg, 2002; Barea *et al.*, 2005; Bohigas and Leboeuf, 2002a,b; Hirsch *et al.*, 2005, 2004; Molinari and Wei-

denmüller, 2006, 2004; Olofsson *et al.*, 2006, 2008), noticeably smaller than shell effects contributions due to periodic orbits and deformations, which are of the order of several MeVs.

The effect of periodic orbits is not limited to finite systems: the Casimir energy in quantum field theory (Casimir, 1948; Klimchitskaya *et al.*, 2009), critical phenomena (Fisher and de Gennes, 1978; Hanke *et al.*, 1998), and strongly interacting infinite inhomogeneous systems, e.g. nuclear pasta phase in neutron stars (Bulgac and Magierski, 2001, 2002; Bulgac *et al.*, 2005, 2006; Magierski *et al.*, 2003; Magierski and Bulgac, 2004b; Magierski and Heenen, 2002b; Yu *et al.*, 2000), can also be explained and calculated to high precision by evaluating the contributions from periodic orbits. This method has become the standard for evaluating the Casimir energy in a variety of fields (Bordag and Pirozhenko, 2010; Canaguier-Durand *et al.*, 2010; Graham, 2014; Rahi *et al.*, 2009; Schaden, 2010).

It is somewhat surprising that shell effects from periodic orbits appear at the same level as deformation effects in the energy of nuclear systems. Naïvely one might expect the deformation energy to be controlled by the surface area of a saturating system, and thus to contribute as a correction to the surface term in nuclear mass formulas like Eqs. (1) and (2). However, the deformation energy in nuclei has a quantum nature, and is determined by a delicate interplay between energy changes induced by the changes in surface area and the shell effects. A similar behavior has been observed in the case of atomic clusters with up to 3000 electrons (Bulgac and Lewenkopf, 1993), leading to the leveling of the peaks, which one would otherwise expect in the absence of deformation), leaving in place only the large negative shell-corrections for the magic spherical systems, as seen in Fig. 4 in case of nuclei.

The shape stability of a many-fermion system is controlled by the single-particle level density at the Fermi level. In an open-shell system this level density is high; the system can thus deform quite easily and single-particle levels can rearrange until the level density is low enough to render the system stable. The stabilization process of the nuclear deformation in the ground state is analogous to the Jahn-Teller effect in polyatomic molecules (Jahn and Teller, 1937), where the high degeneracy of the ground state is lifted by the deformation of the system. This mechanism leads to new “magic numbers” in deformed systems as Strutinsky discussed in his seminal papers (Strutinsky, 1966, 1967, 1968). The increase in surface area and the energy penalty incurred (deformation energy) is canceled to a large extent by the shell-corrections (due to periodic orbits in the deformed potential), unless the system is “magic” or “semi-magic”. This cancellation between deformation energy and shell effects suggests that open-shell systems should be easier to deform than magic systems. This property is consistent with the character of the residuals remaining after the fit of the nuclear binding energies with Bethe-Weizsäcker formulas like Eqs. (1) and (2) and shown in Fig. 1 (see also Fig. 4). The largest residuals appear as large (negative) spikes at the shell closures for spherical nuclei with magic numbers of either protons or/and neutrons, while the expected (positive) peaks in between magic numbers are flattened.

Our goal is to generate a phenomenological nuclear energy density functional (NEDF) with the minimal number of physically motivated parameters required to describe static bulk nuclear properties. This new NEDF may also describe nuclear dynamics in real time.

## II. STATIC PROPERTIES

The lesson from our brief historical review is that, since nuclei are saturating systems with a rather well defined saturation density, the bulk of the nuclear binding energy should be fixed by the geometry of the nuclei (volume, surface area, curvature radius) to sub-percent accuracy. As demonstrated in Table I, the accuracy of the mass formulas Eqs. (1) and (2) – which both lack shell effects, deformation, spin-orbit effects, pairing, etc. – suggests that such a nuclear energy density functional (NEDF) should be capable of describing at a similar level of accuracy both the nuclear binding energies, and the proton and neutron matter density distribution. Therefore, we might reasonably expect that a NEDF will also describe the nuclear charge radii, for which there is a large amount of accumulated data (Angeli and Marinova, 2013). Quantum effects enter at the level of a few MeVs per nucleus, reducing the rms energy error  $\chi_E$  from around 3 MeV to about 0.5 MeV (Moller *et al.*, 1995; Möller *et al.*, 2012), and are most pronounced for magic or semi-magic nuclei, see Fig. 1. The shell corrections will be neglected in this round, but can be added through the Strutinsky procedure (Bohr and Mottelson, 1998; Brack *et al.*, 1972, 1985; Moller *et al.*, 1995; Möller *et al.*, 2012; Myers and Swiatecki, 1974, 1990, 1991, 1996, 1969, 1966; Ring and Schuck, 2004; Strutinsky, 1966, 1967, 1968; Strutinsky and Magner, 1976).

A number of corrective terms might be considered to improve the accuracy of the nuclear mass formulas Eqs. (1) and (2). For example, in the Coulomb term, one might replace  $Z^2$  with  $Z(Z-1)$  to correctly count the number of proton pairs, and one might add an additional term proportional to  $Z$  to account for the Coulomb exchange interaction and screening (Bulgac and Shaginyan, 1996). Motivated by Eq. (4), one might also consider including terms proportional to  $A^{1/3}$  and  $A^0$ . The symmetry energy terms might also be “corrected” by replacing  $(N-Z)^2/4$  with  $T(T+1)$  where  $T = |N-Z|/2$ . Finally, one might introduce an additional correction to account for the Wigner energy  $\propto |N-Z|$ , which appears as a cusp in the nuclear binding energies as a function of  $N-Z$  (basically only for nuclei with  $|N-Z| \leq 2$ ).

However, including these corrections lead to very small improvements in the energy rms  $\chi_E$  beyond the value 2.64 MeV obtained with the main terms of Eq. (2). These corrections are eclipsed by the shell effects as seen in Fig. 1. From the nature of the residuals  $E_{\text{exp}} - E_{\text{th}}$  in Fig. 1 – sharp negative spikes at the magic numbers, but roughly constant fluctuations in between – one can conclude that mass formulas of the type Eq. (2) do encode the role of the nuclear deformation. Shell effects are likely responsible for most of these residuals, and we shall discuss how to include these toward the end of this

paper. A sufficiently accurate theory of nuclear masses may even aim to include contributions arising from quantum chaos.

We will describe a NEDF, which depends on the smallest number of phenomenological parameters to account for all the contributions in the nuclear mass formulas Eqs. (1) and (2), with the exception of the even-odd staggering due to pairing effects. First we relate these parameters to various physical quantities relevant for nuclear physics. For a large nucleus, the Coulomb energy can be used to estimate the saturation density  $\rho_0$  by approximating the nucleus as a uniformly charged sphere with  $E_C = 3Z^2 e^2 / 5R = a_C Z^2 / A^{1/3}$ , where  $R = r_0 A^{1/3}$  and  $r_0 \approx 1.2$  fm is a nuclear length scale:

$$\rho_0 = \frac{3}{4\pi r_0^3}, \quad \text{where} \quad r_0 = \frac{3e^2}{5a_C}. \quad (7a)$$

One can further estimate the ground-state energy of infinite nuclear matter per nucleon  $\varepsilon_0$ , the nuclear surface tension  $\sigma$ , and their dependence on the isospin  $(N - Z)/2$ :

$$\varepsilon_0 = \frac{E(N, Z)}{A} = a_v + a_I \frac{(N - Z)^2}{A^2}, \quad (7b)$$

$$\sigma = a_s + a_I' \frac{(N - Z)^2}{A^2}. \quad (7c)$$

Finally, one can relate the value of the coefficient  $a_C'$  (or of the alternative coefficient of the contribution  $a_C'' Z^2 / A$  to the mass formula (Myers and Swiatecki, 1969)) with the nuclear surface diffuseness.

One thus expects a NEDF as accurate as the mass formula to contain not more than 5 or 6 significant parameters. As we shall see, such a functional does exist, and performs comparably well with as few as 4 parameters however. That a functional dependent on such a small number of phenomenological parameters can go far beyond the capabilities of mass formulae to describe density distributions and dynamics is truly remarkable.

### A. Form of the NEDF

We postulate a NEDF with three main contributions, which significantly improves on the Weizsäcker's original idea (Weizsäcker, 1935):

$$\mathcal{E}[\rho_n, \rho_p] = \mathcal{E}_{\text{kin}}[\rho_n, \rho_p] + \mathcal{E}_C[\rho_n, \rho_p] + \mathcal{E}_{\text{int}}[\rho_n, \rho_p]. \quad (8)$$

As we shall now discuss, the first two terms are well motivated by a semi-classical expansion and electrodynamics and they have no free parameters. All of the phenomenological parameters occur in the interaction piece alone.

*Kinetic Terms:* The kinetic energy density follows from a semi-classical expansion of the non-interacting system (Brack and Bhaduri, 1997; Dreizler and Gross, 1990), and is expressed in

terms of the neutron/proton number densities  $\rho_{n,p}$  and masses  $m_{n,p}$ :

$$\mathcal{E}_{\text{kin}}[\rho_n, \rho_p] = \sum_{\tau=n,p} \frac{\hbar^2}{2m_\tau} \left[ \frac{1}{9} |\nabla \rho_\tau^{1/2}|^2 + \frac{3}{5} (3\pi^2)^{2/3} \rho_\tau^{5/3} \right] + \dots \quad (9)$$

Higher order corrections to this are considered in Eq. (13) below. The factor of  $1/9$  can be derived for smoothly varying densities, and should be compared with the factor of unity originally suggested by Weizsäcker (1935).

*Coulomb Terms:* The direct Coulomb energy and exchange contribution in the Slater approximation are:

$$\mathcal{E}_C[\rho_n, \rho_p] = \frac{1}{2} V_C(\mathbf{r}) \rho_{\text{ch}}(\mathbf{r}) - \frac{e^2 \pi}{4} \left( \frac{3\rho_p(\mathbf{r})}{\pi} \right)^{4/3}, \quad (10a)$$

$$V_C(\mathbf{r}) = \int d^3 r' \frac{\rho_{\text{ch}}(\mathbf{r}')}{|\mathbf{r} - \mathbf{r}'|}, \quad (10b)$$

where  $e$  is the proton charge, and  $\rho_{\text{ch}}$  is the charge density, which is obtained from the proton and neutron densities by convolving with the appropriate charge form factors:

$$\rho_{\text{ch}} = G_E^n * \rho_n + G_E^p * \rho_p. \quad (10c)$$

The charge form factors are determined experimentally, and we approximate the Fourier transforms of the form factors with the dipole term for the proton,  $G_E^p(Q) \approx (1 + Q^2/0.71 \text{ GeV}^2)^{-2}$  (Perdrisat *et al.*, 2007), and  $G_E^n(Q) \approx a(1 + Q^2 r_+^2/12)^{-2} - a(1 + Q^2 r_-^2/12)^{-2}$  with  $r_\pm^2 = r_{\text{avg}}^2 \pm \langle r_n^2 \rangle / 2a$ ,  $\langle r_n^2 \rangle = -0.1147(35) \text{ fm}^2$ ,  $r_{\text{avg}} = 0.856(32) \text{ fm}$ , and  $a = 0.115(20)$  (Gentile and Crawford, 2011). Including these form factors does not significantly improve the mass fits, but improves somewhat the fit of the charge radii. In principle, one might allow the coefficient of the Coulomb exchange term to vary; this is done, for example, in atomic physics to obtain better estimates of the Coulomb exchange energy. We find, however, that fitting the nuclear binding energies leads with high accuracy to the same coefficient presented in Eq. (10a), so we leave it fixed and do not include this as a parameter in our model.

We require our energy density functional to be an isoscalar and include no isospin breaking terms other than those due to the neutron-proton mass difference and the Coulomb interaction. Additional isospin violation due to up and down quark mass differences and electromagnetic effects (Miller *et al.*, 1990, 2006) beyond these two contributions are much smaller and are partly responsible mainly for the Nolen-Schiffer anomaly (Nolen and Schiffer, 1969), to which the screening of the Coulomb exchange also contributes at a comparable level (Bulgac and Shaginyan, 1996).

*Interaction Terms:* All the undetermined parameters of the model appear in the interaction terms. We parameterize these as

$$\mathcal{E}_{\text{int}}(\rho_n, \rho_p) = (\eta - \frac{1}{9}) \sum_{\tau=n,p} \frac{\hbar^2}{2m_\tau} |\nabla \rho_\tau^{1/2}|^2 + \sum_{j=0}^2 \mathcal{E}_j(\rho) \beta^{2j} + \mathcal{E}_{\text{entrain}}(\rho_n, \rho_p), \quad (11a)$$

$$\mathcal{E}_j(\rho) = a_j \rho^{5/3} + b_j \rho^2 + c_j \rho^{7/3}, \quad (11b)$$

where  $\rho$  is the total density, and  $\beta$  is the asymmetry:

$$\rho = \rho_n + \rho_p, \quad \beta = \frac{\rho_n - \rho_p}{\rho_n + \rho_p}. \quad (11c)$$

We include a correction to the gradient term in  $\mathcal{E}_{\text{kin}}$  so that the overall coefficient of the gradient term is  $\eta$ , and up to 9 parameters  $a_j, b_j$ , and  $c_j$  for  $j \in \{0, 1, 2\}$  describing the equation of state for homogeneous nuclear matter. Three of these (for  $j = 2$ ) will be fixed by the equation of state of neutron matter determined in ab initio calculations (see section II.C). Three of the remaining six parameters ( $a_0, c_1$ , and a combination of  $a_1$  and  $b_1$ ) are found to be only marginally significant at the level of changing the energy rms by  $\delta \chi_E < 0.1 \text{ MeV}$ , so that in the end we shall be left with only 4 significant parameters:  $\eta, b_0, c_0$ , and a combination of  $a_1$  and  $b_1$ .

We shall later include an entrainment term  $\mathcal{E}_{\text{entrain}}$  with a single parameter  $\alpha$ , the form and meaning of which will be elucidated in section IV, see Eq. (40). We find this term to have very little significance for the static properties of nuclei, but we will show that it has a pronounced effect on isovector dynamics, such as the giant dipole resonance (GDR) mode. For the moment while we discuss static properties we set it to zero  $\alpha = 0$ . One more parameter,  $\xi$ , will be discussed when we will discuss the computation of shell effects in section IV.B.

The equations that determine the equilibrium densities of a nucleus are obtained by minimizing the energy of a given nucleus  $E(N, Z) = \int d^3r \mathcal{E}[\rho_n, \rho_p]$  with respect to the densities, while constraining the total numbers of neutrons  $N$  and protons  $Z$  with two chemical potentials  $\mu_{n,p}$ :

$$-\eta \frac{\hbar^2}{2m_\tau} \nabla^2 \rho_\tau^{1/2} + U_\tau \rho_\tau^{1/2} = \mu_\tau \rho_\tau^{1/2}, \quad (12a)$$

$$U_\tau = \frac{\partial \mathcal{E}[\rho_n, \rho_p]}{\partial \rho_\tau}, \text{ for } \tau \in \{n, p\}. \quad (12b)$$

## B. Gradient Terms

Weizsäcker (1935) originally introduced the term proportional to gradients of the densities  $|\nabla \rho_\tau^{1/2}|^2$  with a value of  $\eta = 1$  that was later shown to be valid only if the density has small amplitude rapid oscillations (Brack and Bhaduri, 1997; Dreizler and Gross, 1990; Jones and Gunnarsson, 1989). It was later rigorously proven that a semi-classical expansion of the

non-interacting fermions in the extended Thomas-Fermi approximation (the limit of a slowly varying external potential) yields the value  $\eta_{\text{TF}} = 1/9$ , which defines the lowest order gradient contributions in  $\mathcal{E}_{\text{kin}}$  (9) (Brack and Bhaduri, 1997; Dreizler and Gross, 1990; Jones and Gunnarsson, 1989). We treat the coefficient  $\eta$  as a phenomenological parameter since gradient terms can also be generated by interactions (Gebremariam *et al.*, 2010; Negele and Vautherin, 1972, 1975). Fitting the nuclear masses yields values of  $\eta$  close to 0.5, roughly half-way between the semi-classical and Weizsäcker values.

A semi-classical expansion of non-interacting fermions (Brack and Bhaduri, 1997; Dreizler and Gross, 1990) yields the following higher order corrections to  $\mathcal{E}_{\text{kin}}$ , that we have not included in Eq. (9):

$$\mathcal{E}_{\nabla^4}(\rho_n, \rho_p) = \sum_{\tau \in \{n,p\}} \frac{\hbar^2}{2m_\tau} \frac{1}{810(3\pi^2)^{2/3}} f(\rho_\tau), \quad (13)$$

$$f(\rho) = \rho^{1/3} \left[ \left( \frac{\nabla \rho}{\rho} \right)^4 - \frac{27}{8} \left( \frac{\nabla \rho}{\rho} \right)^2 \frac{\nabla^2 \rho}{\rho} + 3 \left( \frac{\nabla^2 \rho}{\rho} \right)^2 \right].$$

This type of correction has been studied in nuclear physics and shown to lead to quite accurate estimates of the kinetic energy density within the extended Thomas-Fermi approximation (Brack *et al.*, 1985, 1976; Brack and Bhaduri, 1997). As within a DFT, such terms can also arise due to the finite range of the interactions in a matter similar to some Skyrme interactions (Gebremariam *et al.*, 2010; Negele and Vautherin, 1972, 1975). However, these terms – even with adjustable parameters – do not significantly change the quality of the mass fits, so we do not consider them in our main analysis. Including them perturbatively in the fit, however, does improve the fit of the charge radii. For example, fitting the overall coefficient reduce the charge radii residual  $\chi_r$  (see details in Section III) from  $\chi_r \approx 0.14 \text{ fm}$  to  $\chi_r \approx 0.09 \text{ fm}$ . Fitting each of the three terms independently further reduces the residuals to  $\chi_r \approx 0.06 \text{ fm}$ . We do not include such fourth-order terms in our functional as they can lead to a complex behavior of the emerging equation for the densities, which can be difficult to rationalize. (See, for example, the analysis of fourth order differential equations arising in case of non-local potentials by Bulgac (1988).) Higher order gradient corrections than Eq. (13) lead to an unphysical behavior of the densities in the classically forbidden regions. The semi-classical expansion has an asymptotic character (Jones and Gunnarsson, 1989). It is known that corrections beyond second order do not always lead to improvements (Jones and Gunnarsson, 1989).

We point out one more property that will be discussed in more detail in section IV: a value of  $\eta = 1/4$  corresponds to a dynamical theory of superfluid neutron and proton pairs. One might naïvely have thought of  $\eta \approx 0.5$  as an effective nucleon pair mass  $m_{\text{eff}} \approx 2m$ , but this leaves the potential  $U_\tau$  wrong by a factor of 2. The parameter  $\eta$  may simply be thought of as a way to control the falloff of the densities in the surface region where the interaction effects are still strong. One should not expect to obtain the correct asymptotic behavior of the

densities far from the nucleus, where the interactions become vanishingly small. The main reason is that DFT is by definition an integral approach, which minimizes globally the energy and not particular local quantities.

A gradient term alone of the form  $|\nabla\rho|^2$  instead of  $|\nabla\rho^{1/2}|^2 = |\nabla\rho|^2/4\rho$  leads to unphysical density profiles, with a discontinuity in  $\nabla\rho$  at a finite radius, beyond which the density vanishes exactly.

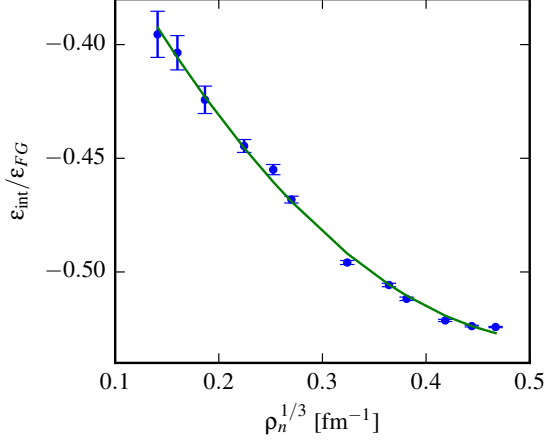


Figure 3 (Color online) The quantum Monte Carlo (QMC) results of Włazłowski *et al.* (2014) for the interaction energy per neutron displayed as the ratio  $\varepsilon_n/\varepsilon_{FG}$  defined in Eq. (15b) (with  $\beta = 1$ ), where  $\varepsilon_{FG} = 3\hbar^2(3\pi^2\rho_n)^{2/3}/(10m_n)$ . If  $a_n = 0$  in Eq. (15b), the ratio  $\varepsilon_{\text{int}}/\varepsilon_{FG}$  would tend to 0 for  $\rho_n \rightarrow 0$ . For densities  $\rho_n^{1/3}|a_{NN}| < 1$  (where  $a_{NN} = 18.9\text{fm}$  is the  $s$ -wave neutron-neutron scattering length) the leading order correction to the kinetic energy density per particle contribution would be instead linear in density  $4\pi\hbar^2 a_{NN}\rho_n/m_n$ .

### C. Infinite Nuclear and Neutron Matter

In infinite homogeneous nuclear matter, as might be found in a neutron star for example, the gradient and Coulomb terms vanish (charge neutrality is maintained by a background of electrons). Neglecting the small neutron-proton mass difference  $m_n \approx m_p = m$ , the functional acquires a simpler form:

$$\mathcal{E}^e(\rho_n, \rho_p) = \frac{3\hbar^2(3\pi^2)^{2/3}}{10m} (\rho_n^{5/3} + \rho_p^{5/3}) + \sum_{j=0}^2 (a_j \rho^{5/3} + b_j \rho^2 + c_j \rho^{7/3}) \beta^{2j}, \quad (14)$$

This portion of the functional is essentially an expansion in powers of the Fermi momenta  $k_F$ :  $k_{n,p} = (3\pi^2\rho_{n,p})^{1/3}$  with three terms only  $k_F^5$ ,  $k_F^6$  and  $k_F^7$ , an ubiquitous power expansion in many-body perturbation theory. It is also supported by fitting

the neutron matter equation of state ( $\rho_p = 0$ ,  $\beta = 1$ ):

$$\varepsilon_n(\rho_n) = \frac{3\hbar^2}{10m_n} (3\pi^2\rho_n)^{2/3} + \varepsilon_{\text{int}}(\rho_n), \quad (15a)$$

$$\varepsilon_{\text{int}}(\rho_n) = a_n \rho_n^{2/3} + b_n \rho_n + c_n \rho_n^{4/3}, \quad (15b)$$

where

$$a_n = a_0 + a_1 + a_2 = -32.6 \text{ MeVfm}^2, \quad (15c)$$

$$b_n = b_0 + b_1 + b_2 = -115.4 \text{ MeVfm}^3, \quad (15d)$$

$$c_n = c_0 + c_1 + c_2 = 109.1 \text{ MeVfm}^4. \quad (15e)$$

These values have been obtained by fitting the neutron matter equation of state as calculated with QMC including up to  $N^3\text{LO}$  two-body and up to  $N^2\text{LO}$  three-body interactions from chiral perturbation theory (Włazłowski *et al.*, 2014), as shown in Fig. 3. Thus, we can include directly the fixed  $j = 2$  parameters  $a_2$ ,  $b_2$ , and  $c_2$  from the values of  $a_n$ ,  $b_n$ , and  $c_n$  describing the QMC results without adding additional free parameters to the NEDF.

As we shall discuss in section III, adding the quartic  $\beta^4$  ( $j = 2$ ) terms does not significantly affect the quality of the mass fits since most nuclei realize small asymmetries  $\beta < 0.25$ . This demonstrates an important point: nuclear masses do not constrain the quartic terms  $\beta^4$ . Higher powers thus provide a direct (and independent) handle on the equation of state of neutron matter.

At this time we do not have an equally accurate QMC calculation of nuclear matter with varying isospin composition, so we must rely instead on a phenomenological approach. Our main assumption is that we can describe both the isoscalar ( $j = 0$ ) and isovector ( $j = 1$ ,  $\beta^2$ ) parts of the nuclear equation of state in a similar fashion to the equation of state of pure neutron matter, using the same three powers of the corresponding Fermi momenta. This approach differs from typical Skyrme-like parameterizations, which include terms with higher powers of densities (e.g.  $\rho^{8/3}$  arising from  $\tau\rho$  type of terms, where  $\tau$  is kinetic energy density).

The terms  $a_j \rho^{5/3}$  are somewhat unexpected and they are not included in Skyrme-like parameterizations. Tondeur (1978) introduced only a term  $a_1$  (without theoretical justification), but it makes sense to include the other  $a_j$  for several reasons. The QMC calculations of Gandolfi *et al.* (2015); Gezerlis and Carlson (2010); and Włazłowski *et al.* (2014), see Fig. 3, are consistent with the existence of a non-vanishing parameter  $a_n$  in the neutron equation of state, which implies that  $a_n = \sum_{j=0}^2 a_j \neq 0$ . They also appear naturally in the case of the unitary Fermi gas (Zwinger, 2012), a fact confirmed to high precision in many experiments. The unitary Fermi gas is a system of two species of fermions, interacting with an  $s$ -wave interaction with zero range and infinite scattering length. In response to the Many-Body X challenge posed by Bertsch in 1999, Baker (1999) showed that the system was stable. The energy density of the unitary Fermi gas scales exactly like the kinetic energy density of a free Fermi gas  $\mathcal{E} \propto \rho^{5/3}$ . Since both neutron and protons have similar  $s$ -wave interaction properties,

one expects the nuclear energy density to behave somewhat like the unitary Fermi gas.

Although the energy density of the unitary Fermi gas scales as the kinetic energy, this is not necessarily due to a mass renormalization as one might naïvely suspect and the answer is not a clear cut one unless additional information is obtained. The QMC calculations of the single quasi-particle dispersion (Carlson and Reddy, 2005) and the calculation of the spectral weight function (Magierski *et al.*, 2011, 2009), both find almost the same effective mass  $\approx m$  in the unitary Fermi gas, very close to unity. However, this does not preclude the interpretation of some part of this term as arising from the kinetic energy density  $\tau$  as is the case in the unitary Fermi gas too (Bulgac, 2007, 2013; Bulgac *et al.*, 2012a). The QMC calculations are not of enough accuracy to either completely exclude or confirm an effective mass different from unity.

Furthermore, QMC calculations of dilute neutron matter at both zero and finite temperatures point to a very large pairing gap  $\Delta \approx 0.25\varepsilon_F$  (Gezerlis and Carlson, 2010) and  $\Delta = 2.8T_c$  (Abe and Seki, 2009a,b; Wlazłowski and Magierski, 2010; Wlazłowski and Magierski, 2011), where  $\varepsilon_F$  and  $T_c$  are the Fermi energy and critical temperature for the superfluid to normal transition. In comparison, Bardeen-Cooper-Schrieffer (BCS) superfluids or mean-field approaches lead  $\Delta \approx 1.76T_c$ , indicating that neutron matter is not a simple BCS superfluid (Magierski *et al.*, 2011, 2009). This is further supported by evidence for a pseudogap at temperatures above  $T_c$  where Cooper pairs and a significant depletion of the density of states still exist even in the absence of long-range order. The properties of neutron matter are thus closely related to those of high  $T_c$  superconductors. The common approach of adding pairing correlations within an Hartree-Fock-Bogoliubov (HFB) or BCS approximation must thus be considered only qualitatively valid, and properly tuned DFT approach is required for quantitative results (Bulgac, 2002, 2007; Bulgac *et al.*, 2014, 2012a, 2011, 2012b; Bulgac and Yoon, 2009; Bulgac and Yu, 2002, 2003; Stetcu *et al.*, 2014, 2011; Wlazłowski *et al.*, 2015; Yu and Bulgac, 2003a,b).

### III. FITTING MASSES AND CHARGE RADII

We fit our NEDFs to the  $N_E = 2375$  measured (not extrapolated) nuclear masses with  $A \geq 16$  from (Audi *et al.*, 2012; Wang *et al.*, 2012). We also consider the  $N_r = 883$  matching charge nuclear radii from (Angeli and Marinova, 2013) with  $\chi_r^2 = \sum |\delta r|^2 / N_r$ . When we include the charge radii in the fit, we minimize the following quantity  $\chi_E^2 / (3 \text{ MeV})^2 + \chi_r^2 / (0.05 \text{ fm})^2$  which roughly equalizes the weight of the mass and radii contributions in the fit.

At this point, we have 7 parameters in our NEDF:  $\eta$ ,  $a_{0,1}$ ,  $b_{0,1}$ , and  $c_{0,1}$  (the  $j = 2$  parameters are fixed by the neutron matter equation of state). In addition, we include by hand the conventional even-odd staggering Eq. (2b) with a coefficient  $\delta$  to describe pairing correlations, even though this has very little significance in the fits. We consider the following fits:

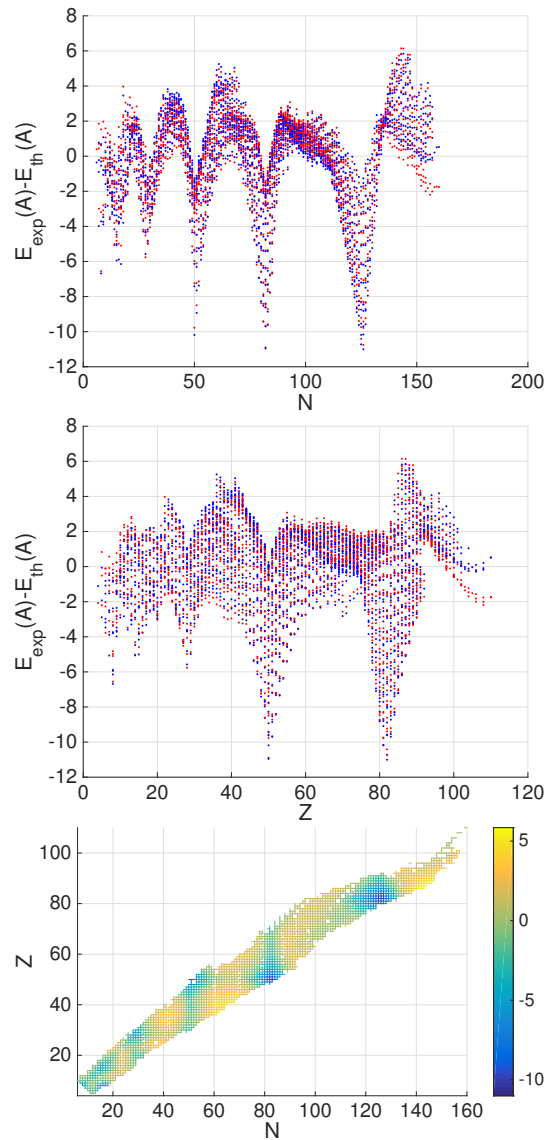


Figure 4 (Color online) The blue dots show the results obtained using fit NEDF-1 with  $\chi_E = 2.58 \text{ MeV}$ , while the red dots are the results of the fits using nuclear mass formula Eq. (2), with  $\chi_E = 2.52 \text{ MeV}$ . When compared against each other, the rms energy deviation between the two fits is  $\chi_E = 0.36 \text{ MeV}$ . Thus, NEDF-1 essentially reproduces the nuclear mass formula Eq. (2). The lower panel is a rendering of calculated ground state energy differences between the experimental measured values and NEDF-1 results, in which one can see clearly the magic numbers separately for neutrons and protons.

**NEDF-0:** A six parameter least-squares fit of the  $N_E = 2375$  nuclear masses (Audi *et al.*, 2012; Wang *et al.*, 2012) including  $\eta$ ,  $b_0$ ,  $c_0$ ,  $a_1$ ,  $b_1$ , and  $\delta$  but setting the nucleon charge form factors Eq. (10c)  $G_E^p \equiv 1$  and  $G_E^n \equiv 0$ .

**NEDF-1:** The same as NEDF-0, but including the measured charge form factors. Comparing with NEDF-0 we see that the electric form factors are not significant for the overall mass fits, but slightly impact the charge radii at the 0.01 fm level (for the reduced  $\chi_r$ ).



NEDF	$\eta$	$\tilde{a}_0$	$\tilde{b}_0$	$\tilde{c}_0$	$\tilde{a}_1$	$\tilde{b}_1$	$\tilde{c}_1$	$\tilde{a}_2$	$\tilde{b}_2$	$\tilde{c}_2$	$\delta$	$\chi_E$ [MeV]	$\chi_r$ [fm]
0	0.4719	0	-3.15166	2.12378	1.048	-0.610	0	0	0	0	0.3246	2.59	0.145
1	0.4742	0	-3.13778	2.10995	0.981	-0.544	0	0	0	0	0.3250	2.58	0.135
2	0.4743	0	-3.14595	2.11873	0.961	-0.521	0	0	0	0	0	2.71	0.140
1r	0.4807	0	-2.98351	1.94501	1.087	-0.668	0	0	0	0	0.3330	2.71	0.051
3	0.4800	-0.088	-2.95408	2.01459	1.000	-0.549	-0.017	0	0	0	0.3234	2.58	0.139
3n	0.4739	-0.061	-3.00477	2.03797	1.565	-1.367	0.181	-1.765	3.8811	-1.9731	0.3279	2.57	0.133
3nr	0.4815	-0.061	-2.86708	1.89073	1.563	-1.347	0.169	-1.763	3.7239	-1.8138	0.3529	2.67	0.050
E	0.4885	0	-3.14903	2.11957	0.277	0.277	0	0	0	0	0.3177	2.64	0.129
Er	0.4957	0	-3.00642	1.96664	0.264	0.264	0	0	0	0	0.3600	2.74	0.051
En	0.4866	0	-3.15157	2.12271	0.272	0.272	0	-0.533	2.3889	-1.8763	0.3192	2.62	0.133
Enr	0.4970	0	-3.00488	1.96492	0.260	0.260	0	-0.521	2.2540	-1.7185	0.3545	2.74	0.051

Table II Dimensionless fit parameters and residuals for the various NEDFs. Parameters have been scaled by appropriate powers of  $\rho_0 = 0.15 \text{fm}^{-3}$  and  $\epsilon_F = \frac{\hbar^2}{2m} (3\pi^2 \rho_0 / 2)^{2/3} = 35.2941961307 \text{MeV}$ :  $\tilde{a}_j = a_j \rho_0^{2/3} / \epsilon_F$ ,  $\tilde{b}_j = b_j \rho_0 / \epsilon_F$ , and  $\tilde{c}_j = c_j \rho_0^{4/3} / \epsilon_F$ .

**NEDF-2:** The same as NEDF-1, but without the pairing parameter  $\delta = 0$ . Comparing with NEDF-1 we see that odd-event staggering is also relatively insignificant at the level of 0.1 MeV per nucleus. This is consistent with the results from the mass formulas in Table I.

**NEDF-1r:** The same as NEDF-1, but including the  $N_r = 883$  charge radii into the fit. We see that there is significant room to improve the description of the charge radii without significantly degrading the mass fits. The charge radii residuals for NEDF-1 and NEDF-1r are plotted in Fig. 8.

**NEDF-3:** The same as NEDF-1, but with all 8 parameters, including  $a_0$  and  $c_1$  that we omitted from the previous fits. In conjunction with the principal component analysis shown in Fig. 11, this fit demonstrates that the terms with parameters  $a_0$  and  $c_1$  are insignificant.

**NEDF-3n:** The same as NEDF-1, but with all 8 parameters, including  $a_0$  and  $c_1$  that we omitted from the previous fits, and the  $\beta^4$  parameters for the terms quartic in isospin, constrained by the QMC neutron matter equation of state (Włazłowski *et al.*, 2014) using Eqs. (15b). That the quality of the fit, isoscalar, and isovector parameters change very little, demonstrates that the neutron matter equation of state is essentially independent of the nuclear masses.

**NEDF-3nr:** The same as NEDF-3n but including the charge radii as in fit NEDF-1r. That the  $a_0$  and  $c_1$  terms are insignificant for both masses and radii is also emphasized by this fit.

Finally, we consider two parameter sets that represent the minimal functionals. Each has 4 significant parameters (and  $\delta$ , which is insignificant):

**NEDF-E:** Following the principal component analysis of NEDF-3n (discussed below) we find the combination  $a_1 - b_1 \rho_*^{1/3}$  to be only weakly constrained by the mass fit.

To test this, we set  $a_1 = b_1 \rho_*^{1/3}$  where  $\rho_* = 0.15 \text{fm}^{-3}$  is a constant. The combination  $a_1 - b_1 \rho_*^{1/3}$ , to which the masses are insensitive, allows independent control the slope  $L_2$  of the symmetry energy (see Eq. (32e)). From the fits we see that this same combination also controls the neutron skin thicknesses.

**NEDF-Er:** The same as NEDF-E but including the charge radii as in fit NEDF-1r.

**NEDF-En:** This is our main fit. It is the same as NEDF-E but includes the  $\beta^4$  parameters adjusted to reproduce the neutron matter equation of state as in fit NEDF-3n.

**NEDF-Enr:** The same as NEDF-En but including the charge radii as in fit NEDF-1r.

These fits are summarized in Table II with the saturation and symmetry properties in Table III. The residuals for fit NEDF-1 are shown in Fig. 4 and compared with a fit to the nuclear with mass formula Eq. (2).

The reduced  $\chi_E$  for these fits is comparable to that obtained using the nuclear mass formulas Eq. (1) with 4 parameters (plus  $\delta$ ) and Eq. (2) with 5 parameters (plus  $\delta$ ). This is consistent with our hypothesis that a NEDF for masses should contain no more than 5 significant parameters. Note, however, that unlike the mass formulas, the NEDF also gives a good description of charge radii – for which the mass formula says nothing – and provides access to nuclear dynamics as we shall discuss in section IV.

## A. Discussion

The accuracy of the ground state binding energies obtained using this NEDF, see Fig. 4 and Table II, compares extremely well with much more sophisticated self-consistent approaches that naturally account for the shell-corrections.

The UNEDF2 nuclear energy functional introduced by Kortelainen *et al.* (2014a,b) has a residual of  $\chi_E = 1.95 \text{MeV}$

per nucleus for 555 even-even nuclei. Since the UNEDF2 functional is formulated in terms of single-nucleon orbitals, one would expect it to account for shell-corrections, but this functional still displays large discrepancies of the binding energies of magic nuclei (close to 8 MeV in case of  $^{208}\text{Pb}$ ). The UNEDF2 functional depends on 11 parameters, with several additional parameters to describe pairing correlations. The UNEDF2 functional also leads to a larger pairing coupling constant for protons than for neutrons, thus violating isospin invariance and the expectation that Coulomb effects reduce proton pairing, an expectation which appears to agree with experiments (Lesinski *et al.*, 2009). A natural solution might be to include in the NEDF a pairing contribution of the form

$$\mathcal{E}_{\text{pairing}} = g_0(\rho_n, \rho_p) [|\mathbf{v}_n|^2 + |\mathbf{v}_p|^2] + g_1(\rho_n, \rho_p) [|\mathbf{v}_n|^2 - |\mathbf{v}_p|^2] [\rho_n - \rho_p], \quad (16a)$$

$$g_{0,1}(\rho_n, \rho_p) = g_{0,1}(\rho_p, \rho_n), \quad (16b)$$

where  $\mathbf{v}_{n,p}$  are the anomalous neutron and proton densities respectively. Since in measured nuclei one has predominantly  $N \geq Z$ , see Fig. 7, a phenomenological analysis that leads to an apparent coupling for protons larger than the one for neutrons can be reconciled with coupling constants  $g_0(\rho_n, \rho_p) < 0$  and  $g_1(\rho_n, \rho_p) > 0$ .

Baldo *et al.* (2013, 2008) introduced an energy density functional based on information extracted from QMC calculations of neutron and symmetric nuclear matter, and a few additional parameters to describe pairing and spin-orbit interaction and finite range effects; they assume that no quartic terms in isospin  $\beta^4$  are present in the NEDF. Depending on how they fit various subsets of about 580 nuclei, they find  $\chi_E$  ranging from 1.3 MeV to 2.4 MeV.

Goriely *et al.* (2009, 2013) have produced over the years a series of NEDF in which they obtain an even lower  $\chi_E$  throughout the entire mass table as low as 0.5 MeV. However this was obtained by adding a number of phenomenological corrections, a procedure which so far has not been adopted by the other practitioners using microscopic approaches.

Within relativistic mean-field theory (RMFT) of nuclei in one of the best parametrizations of the NEDF for nuclear masses (Agbemava *et al.*, 2014; Niksic *et al.*, 2011) one achieves a  $\chi_E$  between 2 and 3 MeV for even nuclei using the AME2012 data set (Audi *et al.*, 2012; Wang *et al.*, 2012).

## B. Neutron Matter

The inclusion of the  $j = 2$  terms quartic in  $\beta^4$  in fits NEDF-3n and NEDF-3rn demonstrates an important point: the equation of state of neutron matter has very little impact on the form of the NEDF at the level of quadratic isovector contributions (see also the previous section). We have attempted to perform a fit of the nuclear binding energies by including the quadratic terms in  $\beta$  only, defining the coefficients of the functional through the neutron equation of state ( $a_1 = a_n - a_0$ ,  $b_1 = b_n - b_0$ , and  $c_1 = c_n - c_0$ ), and allowing  $\eta$ ,  $a_0$ ,  $b_0$ , and  $c_0$  to vary. The energy rms was at best  $\chi_E = 4.36$  MeV.

In measured nuclei, the ratio  $\beta = (\rho_n - \rho_p)/\rho \approx (N - Z)/A$  is  $|\beta| < 0.25$  (with a very small number of exceptions), hence nuclear masses are essentially insensitive to the presence of the  $\beta^4$  terms, as  $|\beta|^4 < 1/256$ . Only 46 nuclei have  $|N - Z|/A > 1/4$  (mostly with  $A < 50$ ) and only 68 nuclei have  $N \leq Z$  in the set we consider. To assess the magnitude of these effects, we have evaluated the  $\beta^4$  contributions to the nuclear binding energies perturbatively, see Fig. 5. This contribution is quite small and can be easily overlooked when discussing known nuclei, but is crucial in order to correctly reproduce the energy of neutron matter.

Thus, using properties of the neutron matter to constrain the form of the NEDF and/or arguing against the inclusion of higher powers of  $(\rho_n - \rho_p)$  (Baldo *et al.*, 2013, 2008; Brown, 2013; Brown and Schwenk, 2014; Eler *et al.*, 2013; Fantina *et al.*, 2014; Fayans, 1998; Goriely *et al.*, 2013; Reinhard and Nazarewicz, 2010) is an ill-advised procedure, and the applications of functionals constructed in this manner, in particular to star environments, should be regarded with suspicion.

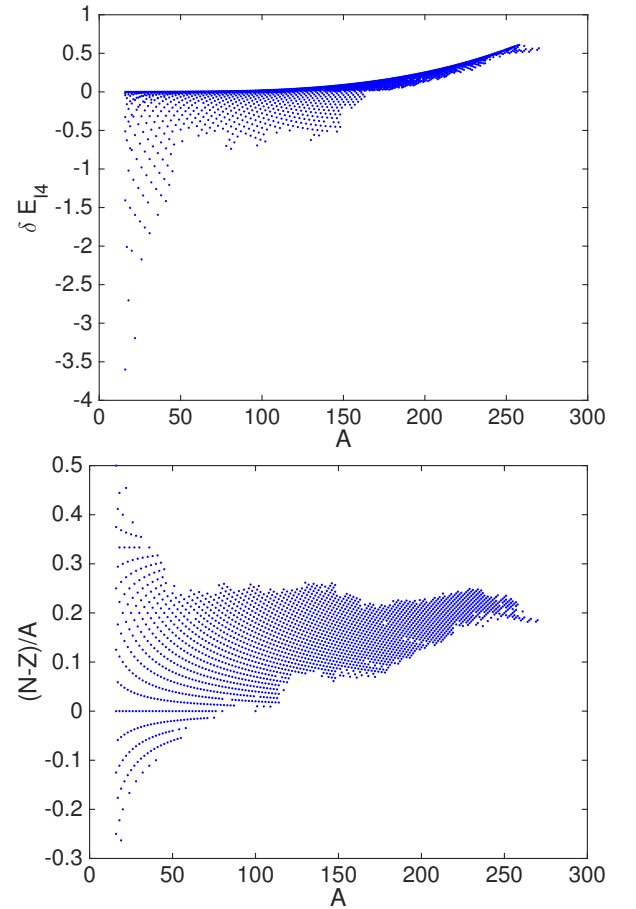


Figure 5 (Color online) The contribution to the ground state energies of the terms quartic in isospin density  $\delta E_{I4} = \int d^3 \mathcal{E}_2(\rho) \beta^4$ , evaluated perturbatively with NEDF-1, see Table II. In the lower panel we display the ratio  $(N - Z)/A$  for the nuclei we have considered. Among the 2375 nuclei we have considered, there are 33 nuclei with  $N = Z$ , 78 nuclei with  $Z > N$ , and 70 nuclei with  $|N - Z|/A > 1/4$ .

NEDF	$\rho_0$ [fm <sup>-3</sup> ]	$-\varepsilon_0$	$K$	$S$	$L$	$L_2$	Neutron skin	
							<sup>208</sup> Pb [fm]	<sup>48</sup> Ca [fm]
0	0.136	15.24	222.5	26.8	34.1	32.8	0.082	0.118
1	0.136	15.22	222.4	26.7	35.9	34.7	0.087	0.123
2	0.136	15.21	222.2	26.7	36.8	35.6	0.089	0.125
1r	0.148	15.48	227.7	27.1	30.9	29.6	0.078	0.116
3	0.136	15.21	216.5	26.7	34.7	33.4	0.088	0.124
3n	0.137	15.20	218.2	30.0	29.3	16.7	0.068	0.107
3nr	0.147	15.44	222.9	31.0	31.2	15.5	0.068	0.107
E	0.136	15.28	223.1	29.7	68.2	66.9	0.159	0.174
Er	0.147	15.53	228.1	30.6	70.2	68.9	0.161	0.176
En	0.136	15.27	222.9	30.1	29.1	66.1	0.152	0.172
Enr	0.147	15.53	228.2	31.1	31.1	68.3	0.156	0.174

Table III Saturation, symmetry, and neutron skin properties for the various NEDFs. All values in MeV unless otherwise specified.

### C. Saturation and Symmetry Properties

The isoscalar parameters  $j = 0$  and quadratic isovector parameters  $j = 1$  ( $\beta^2$ ) may be directly related to the saturation and symmetry properties respectively by expanding the energy per nucleon of homogeneous nuclear matter Eq. (14) about the symmetric saturation point  $\rho_n = \rho_p = \rho_0/2$ :

$$\frac{\mathcal{E}(\rho_n, \rho_p)}{\rho} = \varepsilon_0(\rho) + \varepsilon_2(\rho)\beta^2 + \varepsilon_4(\rho)\beta^4 + \mathcal{O}(\beta^6). \quad (17)$$

The saturation density  $\rho_0$ , energy per nucleon  $\varepsilon_0$ , and incompressibility  $K_0$  are then defined by the minimum  $\varepsilon'_0(\rho_0) = 0$ , and depend only on the  $j = 0$  isoscalar parameters  $a_0$ ,  $b_0$ , and  $c_0$ . Expanding about  $\rho_0$  in  $\delta = (\rho - \rho_0)/3\rho_0$  and in powers of  $\beta = (\rho_n - \rho_p)/\rho$ , one can define various “local” contributions to the symmetry energy  $S_{2,4}$ , its density dependent slope  $L_{2,4}$ , etc.:

$$\begin{aligned} \varepsilon_0(\rho) &= \varepsilon_0 + \frac{1}{2}K_0\delta^2 + \mathcal{O}(\delta^3), \\ \varepsilon_2(\rho) &= S_2 - L_2\delta + \frac{1}{2}K_2\delta^2 + \mathcal{O}(\delta^3), \\ \varepsilon_4(\rho) &= S_4 - L_4\delta + \frac{1}{2}K_4\delta^2 + \mathcal{O}(\delta^3) \end{aligned} \quad (18)$$

Since we include also quartic terms  $\beta^4$ , we must differentiate between these local symmetry parameters  $S_2$ ,  $L_2$ , etc. and the full symmetry parameters defined as the difference between symmetric matter and pure neutron matter (see also the discussion of Lattimer (2014)):

$$S = \frac{\mathcal{E}(\rho_0, 0) - \mathcal{E}(\rho_0/2, \rho_0/2)}{\rho_0}, \quad (19)$$

$$L = 3\rho \frac{d}{d\rho} \left( \frac{\mathcal{E}(\rho, 0)}{\rho} \right) \Big|_{\rho_0} = 3\rho_0 \varepsilon'_n(\rho_0). \quad (20)$$

where  $\varepsilon_n\rho$  is the neutron equation of state (15a). Since the saturation density  $\rho_0$  minimizes the energy of symmetric matter, the slope of the full symmetry energy  $L$  at  $\rho_0$  depends only on the equation of state of pure neutron matter. Thus, the QMC neutron equation of state alone fixes the global density

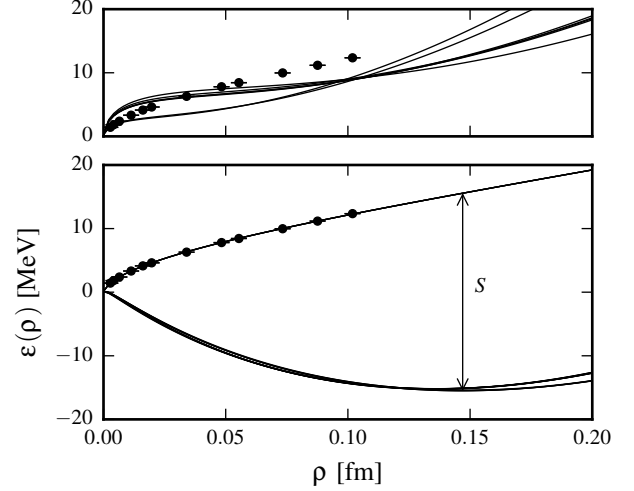


Figure 6 (Color online) Equation of state of symmetric nuclear matter (all functionals) and neutron matter (for NEDF-3n, 3nr, En, Enr only) in the lower panel and pure neutron matter (upper panel) for NEDF-0, 1, 1r, 2, 3, E, and Er (which do not constrain the neutron equation of state and have only  $\beta^2$  contributions). The black dots shows the QMC results (Włazłowski *et al.*, 2014). The symmetry energy  $S$  is indicated for the functionals NEDF-Er and Enr. The slope  $L \approx 30$  MeV is fixed by the neutron matter equation of state alone (if used as a constraint, see Eq. (20)). In this case the slope  $L_2/3\rho_0$  may be tuned without significantly affecting the mass fit by adjusting the insensitive combination  $a_1 - b_1\rho_*^{1/3}$ , see Section III.G. Functionals with only quadratic isospin contributions ( $\beta^2$ ) appear to cross near  $\rho_n \approx 0.1$  fm<sup>-3</sup> (upper panel).

dependence of the symmetry energy  $L = 3\rho_0 \varepsilon'_n(\rho_0) \approx 30$  MeV. (Small variations in  $L$  seen in Table III for functionals fitting neutron matter are due to the variations in  $\rho_0$  from fit to fit.)

When only  $\beta^2$  isospin contributions are included in the functional, our fits to the nuclear binding energies display a feature reported in other NEDFs: the energy per neutron in pure neutron matter appears to be well constrained at a density of  $\rho_n \approx 0.1$  fm<sup>-3</sup> where all functionals cross, see Fig. 6. However, the value for the energy per neutron  $\approx 9$  MeV at this point in our fits is significantly smaller than the value  $\approx 12.35$  MeV obtained in QMC calculations of Włazłowski *et al.* (2014). This feature is not present when the  $\beta^4$  terms are included (NEDF-3n, NEDF-3nr, NEDF-En and NEDF-Enr) and the QMC results are reproduced without significantly affecting the mass fits. The statement often made in the literature (see Horowitz *et al.* (2014a) and references therein) that the value of the symmetry energy at  $\rho \approx 0.1$  fm<sup>-3</sup> is well constrained by nuclear masses must only be applied to the local expansion  $S_2$  at this density, but not to the symmetry energy difference  $S$  between symmetric and pure neutron matter.

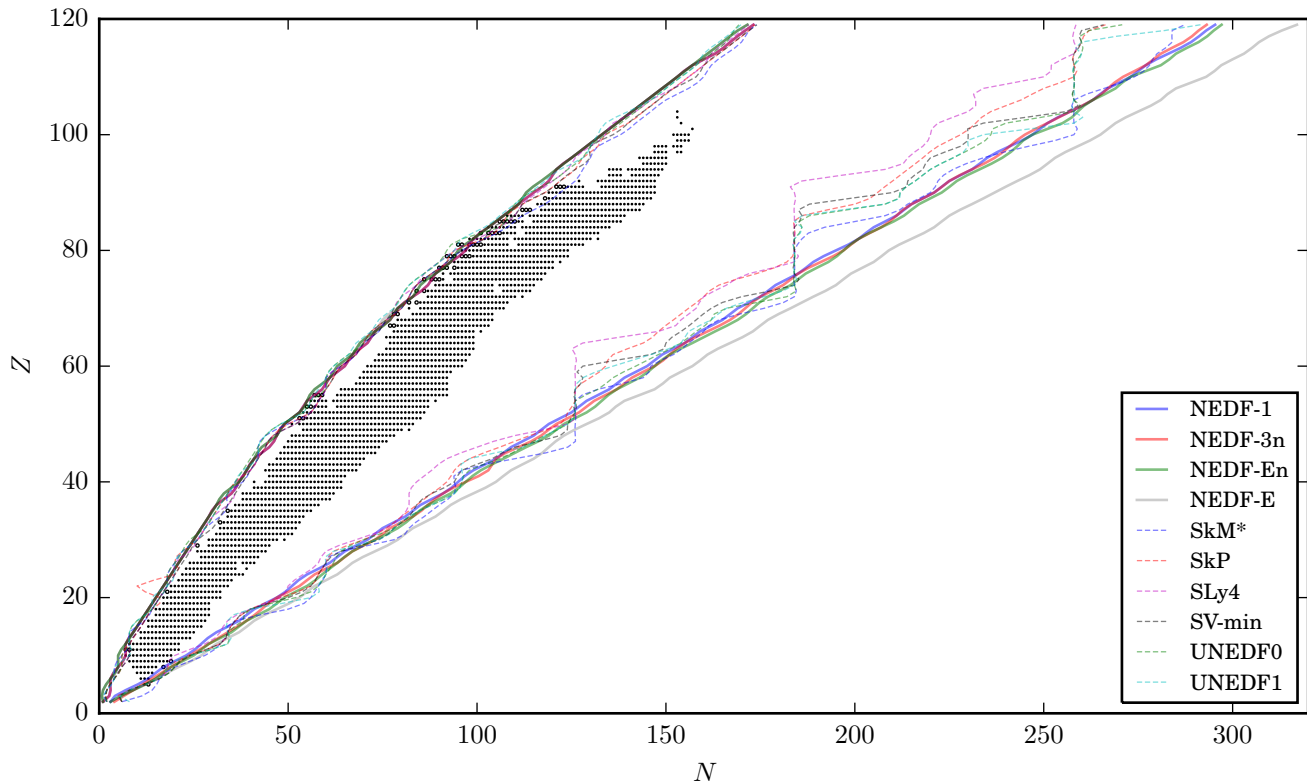


Figure 7 (Color online) The proton and neutron driplines evaluated with NEDF-1, NEDF-3n, NEDF-E and NEDF-En compared with those predicted by fully self-consistent calculations using SkM\*, SkP, SLy4, SV-min, UNEDF0, and UNEDF1 (Erler *et al.*, 2012). The 2375 nuclear masses from (Audi *et al.*, 2012; Wang *et al.*, 2012) are displayed as dots and nuclei unstable with respect to the emission of a single proton or neutron are denoted with open circles. NEDF-E leads to a neutron dripline shifted quite a bit away from the other predictions. This is due to changing  $L_2$  to a value of the neutron skin thickness in  $^{208}\text{Pb}$  consistent with experiment, see Table III, but inconsistent with the neutron equation of state and the values for  $S$  and  $L$ , which appear to control the position of the dripline.

#### D. Symmetry Energy and Neutron Skin Thickness

As shown in Table III, the binding energy of nuclear matter and the symmetry energy predicted by all NEDFs fits agrees well with the value obtained with the mass formula (2). Our fits generally estimate the slope of the symmetry energy  $L_2$  from 29 MeV to 36 MeV, but NEDF-E, NEDF-En, NEDF-Er, and NEDF-Enr demonstrate that this is essentially unconstrained by the masses and can be adjusted independently with the combination  $a_1 - b_1\rho_*^{1/3}$ .

We also compute the neutron skin thickness of  $^{48}\text{Ca}$  and  $^{208}\text{Pb}$ , for which precision measurements CREX and PREX<sup>1</sup> are underway, see (Horowitz *et al.*, 2014b) for details. For NEDF-1 through NEDF-3rn, the neutron skin of  $^{208}\text{Pb}$  ranges from 0.07 fm to 0.09 fm while the  $^{48}\text{Ca}$  skin ranges from 0.106 fm to 0.125 fm. The  $^{208}\text{Pb}$  neutron skin appears quite a bit thinner than a recent measurement of 0.15(3) fm (Tarbert

*et al.*, 2014), but the results of NEDF-E, NEDF-Er, NEDF-En, and NEDF-Enr demonstrate that this is also controlled by the same combination  $a_1 - b_1\rho_*^{1/3}$  as  $L_2$ , and hence unconstrained by the masses.

Since the slope of the symmetry energy  $L = L_2 + L_4 + \dots \approx 30$  MeV is fixed by the neutron matter equation of state, requiring a larger value of  $L_2 \approx 60$  MeV to explain the neutron skin thickness of  $^{208}\text{Pb}$  also suggests that at least quartic terms are required in the functional.

#### E. Neutron Drip Line

It is interesting to compare the limits of nucleon stability predicted by our NEDFs. In Fig. 7 we compare the proton and neutron drip lines obtained with our NEDF-1, 3n, E, and En against the predictions of UNEDF0 and UNEDF1, as well as those obtained with other Skyrme parametrizations extracted from the supplemental data of Erler *et al.* (2012). It is a bit unexpected that NEDF-1 and NEDF-3n and En have almost identical neutron driplines considering that NEDF-1 and E have only quadratic isovector contributions, while NEDF-3n

<sup>1</sup> Proposals and related information available at <http://hallaweb.jlab.org/parity/prex>

and  $E_n$  also have quartic terms constrained by the neutron matter equation of state. Apparently these quartic terms – and therefore the neutron equation of state – play a minor role even in nuclei with a very large neutron excess  $N - Z \approx 160$  when  $(N - Z)/A \approx 0.4$  since  $[(N - Z)/A]^4 \approx 0.0256$  is small.

The proton driplines are in good agreement with other NEDFs (up to odd-even effects), even though our NEDFs lacks quantum effects. Our NEDFs suggest that the neutron dripline may extend somewhat further than for conventional functionals. If significantly more nuclei are stable against nucleon decay, this may dramatically impact the astrophysical  $r$ -process, which is predicted to follow lines of constant separation energy in close proximity to the neutron dripline (Langake and Wiescher, 2001; Meyer, 1989). Meyer (1989) considered neutron star ejecta as the site of  $r$ -process nucleosynthesis, and determined that the reaction flow is very close to the dripline. Even though his simulations were performed for relatively cold matter (recent simulations seem to indicate that the star material is somewhat heated (Goriely *et al.*, 2011; Rosswog *et al.*, 2014)), it will be interesting to simulate the  $r$ -process using the present NEDFs. There are almost 9000 nuclei between the proton and neutron driplines in case of NEDF-1 and NEDF-3n, most of which might be stable against nucleon decay (quantum effects are neglected in this estimate). This number is noticeably larger than the estimate  $6900 \pm 500$  obtained in Ref. (Erler *et al.*, 2012). The functionals NEDF-E and NEDF-Er lead to a neutron dripline which is shifted much further, but when the neutron equation of state is incorporated in NEDF-En and NEDF-Enr, the neutron dripline is again very close to the previous position given by NEDF-1 and NEDF-3n. Unlike the neutron skin thickness, which is controlled by  $L_2$ , the position of the neutron dripline appears to be controlled by the full symmetry energy  $S$  and its density dependence  $L$ .

The predicted position of the neutron dripline will likely affect the structure of the neutron star crust inferred from older studies (Baym *et al.*, 1971; Bulgac and Magierski, 2001, 2002; Magierski and Bulgac, 2004a; Magierski *et al.*, 2003; Magierski and Heenen, 2002a; Magierski and Bulgac, 2004b; Negele and Vautherin, 1973). The corresponding increase in the neutron skin thickness will also affect the profile and the pinning energy of quantized vortices in the neutron star crust (Avogadro *et al.*, 2007, 2008; Bulgac *et al.*, 2013; Pizzochero *et al.*, 1997; Pizzochero, 2007, 2011; Yu and Bulgac, 2003c).

Fusion cross sections (Adelberger *et al.*, 2011; Gasques *et al.*, 2005) will also be significantly altered, particularly in stellar environments where neutron rich nuclei fuse via pycnonuclear reactions (Afanasjev *et al.*, 2012; Schram and Koonin, 1990), and where the neutron gas surrounding nuclei leads to their swelling (Umar *et al.*, 2015). A thicker neutron skin with further enhance this effect.

## F. Charge Radii

Using the parameters determined from the mass fits, the NEDF also models the neutron and proton densities in the nuclei,

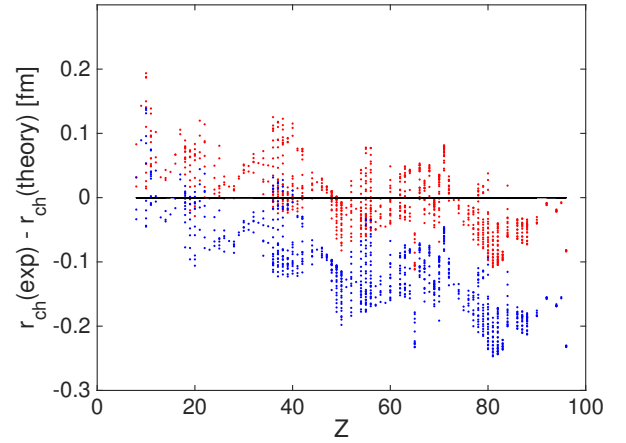


Figure 8 (Color online) The difference between the measured (Angeli and Marinova, 2013) and computed charge radii of 883 nuclei evaluated with NEDF-1 (blue) and NEDF-1r (red), see Table I. The energy rms corresponding to the blue and red points are 2.58 MeV with NEDF-1 and 2.71 MeV with NEDF-1r. The charge radii rms are in these cases 0.135 fm with NEDF-1 and 0.051 fm with NEDF-1r respectively.

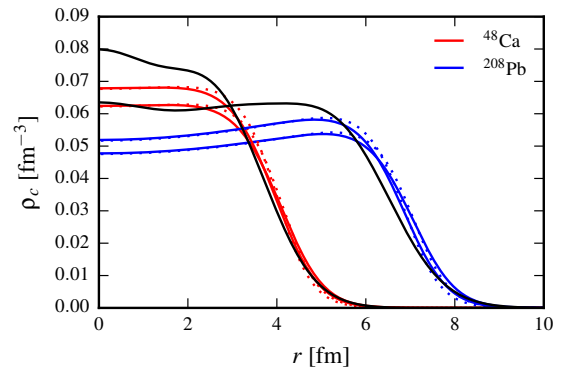


Figure 9 (Color online) The calculated proton  $\rho_p(r)$  (dotted) and charge  $\rho_{ch}(r)$  (solid) densities for  $^{48}\text{Ca}$  (red) and  $^{208}\text{Pb}$  (blue), calculated with NEDF-En (lower curves) and NEDF-Enr (upper curves) compared to charge densities (black) extracted from electron scattering experiments (De Vries *et al.*, 1987).

allowing us to extract the charge radii for the 883 nuclei in (Angeli and Marinova, 2013) that intersect with the 2375 nuclear masses we fit from (Audi *et al.*, 2012; Wang *et al.*, 2012). Without any further adjustment, the NEDF gives an rms residual for these charge radii of  $\chi_r = 0.135$  fm. Including them in the fit (NEDF-1r, NEDF-3nr, and NEDF-Enr) improves this to  $\chi_r = 0.05$  fm without significantly affecting the quality of the mass fits. To compare, fully self-consistent RMFT models realize  $\chi_r$  from 0.023 fm to 0.041 fm (Agbemava *et al.*, 2014; Niksic *et al.*, 2011) depending on the set of nuclei examined.

The differences between the calculated and measured charge radii (Angeli and Marinova, 2013) are illustrated in Fig. 8. In Fig. 9 we compare the proton and charge densities of  $^{48}\text{Ca}$  and  $^{208}\text{Pb}$  calculated with NEDF-E and NEDF-Er with the

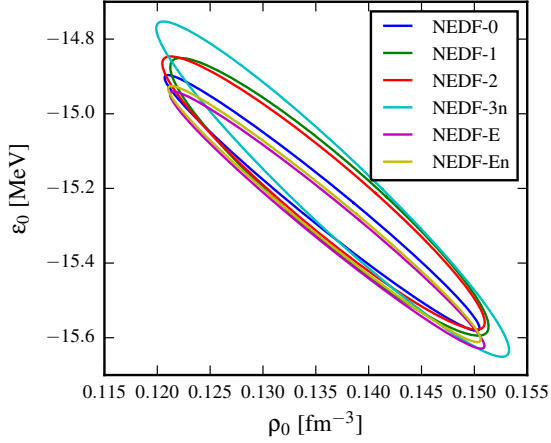


Figure 10 (Color online) The various ellipses show the region in the  $(\epsilon_0, \rho_0)$  plane, in which the NEDF parameters can be changed and to lead to changes in the residual  $\delta\chi_E < 0.2 \text{ MeV}$ . While the equilibrium energy  $\epsilon_0$  and density  $\rho_0$  are controlled mainly by the combination  $\tilde{b}_0 + \tilde{c}_0$ , which is constrained with very high precision, the combination  $\tilde{b}_0 - \tilde{c}_0$  remains significantly less constraint, see Section III.G. This aspect allows us to manipulate to a certain degree the saturation properties, while affecting the overall fit only slightly.

the charge densities extracted from electron scattering experiments (De Vries *et al.*, 1987). The calculated charge density  $^{208}\text{Pb}$  has a slightly larger radius and slightly smaller diffuseness compared to those extracted from data. There may be several ways to cure this deficiency. The nuclear saturation density is not well constrained by the mass fits, and our values appear somewhat low. However, one can constrain the equilibrium density to a value closer to  $\rho_0 = 0.16 \text{ fm}^{-3}$  without affecting the mass fit greatly, see Fig. 10. The surface properties are controlled by the parameter  $\eta$ , and although a single parameter is sufficient to fit the masses, one might introduce a density dependence  $\eta \rightarrow \eta_0 + \eta_1 \rho^{1/3} + \dots$  or even an isospin density dependence to better fit the densities.

We do not have yet a clear understanding of why the light nuclei have slightly smaller radii, while the large nuclei show the opposite behavior, and whether this aspect is correlated with the nuclear surface diffuseness. Within the present approach all nuclei are spherical; quantum effects may have a noticeable impact on the calculated charge radii, but so far we do not know how to disentangle the roles of the bulk and shell-correction effects on these values as cleanly as we do in the case of binding energies.

In order to compare our results with the experimental values of the charge radii, we must correct for the motion of the center of mass, but we find these corrections to be small. In mean-field-like calculations, the center-of-mass of the system moves in the self-consistent potential and one needs to account for these fluctuations before comparing with experimental data. For small nuclei, it is common to treat these center-of-mass fluctuations by assuming that the center-of-mass sits in a harmonic oscillator potential, with the frequency related to the

average curvature of self-consistent nuclear mean-field potential (Lipkin, 1958; Negele, 1970). The calculated charge radius would then be smeared by convolving with the gaussian center-of-mass wavefunction, and the correction implemented as a de-convolution which amounts to the subtraction

$$\langle r_c^2 \rangle = \int d^3r r^2 \rho_c(\mathbf{r}) - \frac{3}{2} \frac{\hbar}{Am\omega} \quad (21)$$

$$\approx \int d^3r r^2 \rho_c(\mathbf{r}) - A^{-2/3} 1.8 \text{ fm}^2, \quad (22)$$

where  $\hbar\omega \approx 1.85 \text{ MeV} + A^{-1/3} 35.5 \text{ MeV}$  approximates the harmonic-oscillator energy (Negele, 1970). (In the full calculation, the charge form factors are included in a similar manner by subtracting the proton and neutron charge radius.) A similar correction of  $\frac{3}{4}\hbar\omega$  should be subtracted from the binding energy of the nucleus. This prescription is expected to be accurate enough for light nuclei, but it is not clear that the harmonic approximation of the mean-field potential will be valid for large nuclei, which saturate to approximately  $\rho_0$  in the core. (Due to the effect of the nuclear surface tension the nuclei are compressed a bit, but at the same time Coulomb repulsion tends to deplete the central charge density.) Here we argue that, for large nuclei, this correction due to the center-of-mass fluctuation is small enough to be discarded (an argument made also by Negele (1970) for large nuclei).

To simplify the following argument, we neglect the proton-neutron mass difference; in actual calculations we use the experimentally measured nucleon masses. The intrinsic radius of a nucleus  $r_{\text{rms}}$  is the expectation value of the square of the distance of the nucleons from the center of mass:

$$r_{\text{rms}}^2 = \frac{1}{A} \sum_{k=1}^A \langle (\mathbf{r}_k - \mathbf{R})^2 \rangle = \frac{1}{A} \sum_{k=1}^A \langle r_k^2 \rangle - \langle \mathbf{R}^2 \rangle = r_m^2 - \langle \mathbf{R}^2 \rangle \quad (23)$$

where  $\mathbf{R} = \sum_k \mathbf{r}_k / A$  is the center-of-mass coordinate and  $\sqrt{r_m^2}$  is the rms mass radius of the nucleus calculated directly within the meanfield theory. This makes it clear that the center-of-mass correction – the second term – is a measure of the size of the center-of-mass fluctuations

$$\begin{aligned} \langle \mathbf{R}^2 \rangle &= \frac{1}{A^2} \left\langle \sum_{k=1}^A r_k^2 + \sum_{k \neq l}^A \mathbf{r}_k \cdot \mathbf{r}_l \right\rangle \\ &= \frac{r_m^2}{A} + \frac{1}{A^2} \left\langle \sum_{k \neq l}^A \mathbf{r}_k \cdot \mathbf{r}_l \right\rangle. \end{aligned} \quad (24)$$

The last term in Eq. (24) is the value of a two-body observable and in Hartree-Fock approximation only the exchange term contributes. Using the known expression for the two-body density in the Hartree-Fock approximation

$$\rho_2(x, y) = \rho_1(x, x)\rho_1(y, y) - \rho_1(x, y)\rho_1(y, x), \quad (25)$$

where  $\rho_1(x, y) = \rho_1(\mathbf{r}_1, \sigma_1, \tau_1, \mathbf{r}_2, \sigma_2, \tau_2)$  is the one-body density matrix. We now approximate this using the Thomas-Fermi

approximation for the density matrix

$$\rho_1(x, y) = \delta_{\sigma_1, \sigma_2} \delta_{\tau_1, \tau_2} \int_{k \leq k_F} \frac{d^3 k}{(2\pi)^3} \exp(i\mathbf{k} \cdot \mathbf{s}), \quad (26)$$

where  $k_F$  is the local neutron or proton Fermi momentum and  $\mathbf{s} = \mathbf{r}_1 - \mathbf{r}_2$ , one can show that

$$\frac{1}{A^2} \left\langle \sum_{k \neq l}^A \mathbf{r}_k \cdot \mathbf{r}_l \right\rangle = -\frac{r_m^2}{A} + \mathcal{O}(A^{-1}). \quad (27)$$

Thus, the leading order terms of the direct and exchange contributions cancel exactly leaving  $\langle \mathbf{R}^2 \rangle = \mathcal{O}(A^{-1})$ , which is significantly smaller than the correction suggested by the harmonic oscillator assumption (Lipkin, 1958; Negele, 1970). We therefore neglect these correction in our fits as they are insignificant in comparison with missing shell effects etc.

It is instructive to perform a similar calculation for the kinetic energy of the center-of-mass

$$\begin{aligned} E_{\text{cm}} &= \frac{1}{2mA} \langle \mathbf{P}^2 \rangle = \frac{1}{2mA} \left\langle \left( \sum_{k=1}^A \mathbf{p}_k \right)^2 \right\rangle \\ &= \frac{\hbar^2}{2mA} \left\langle \sum_{k=1}^A |\nabla \psi_k(\mathbf{r})|^2 \right\rangle + \frac{1}{2mA} \left\langle \sum_{k \neq l} \mathbf{p}_k \cdot \mathbf{p}_l \right\rangle, \end{aligned} \quad (28)$$

(For clarity we have suppressed spin and isospin indices.) Using again the Thomas-Fermi approximation (26), and including the Weizsäcker correction (Brack and Bhaduri, 1997; Dreizler and Gross, 1990; Weizsäcker, 1935) to the kinetic energy density in the direct term, we determine that

$$E_{\text{cm}} \sim \frac{\hbar^2}{2mA} \int d^3 r \left( \nabla \rho^{1/2}(\mathbf{r}) \right)^2 \sim \frac{\hbar^2}{2mr_0^2} A^{-1/3} \quad (29)$$

where  $m$  is a nucleon mass,  $R = r_0 A^{1/3}$  is the nuclear radius, and  $\hbar^2/2mr_0^2 \sim 35 \text{ MeV}$  is of the order of the Fermi energy.

The arguments presented here on the role of center-of-mass fluctuations are based on a Hartree-Fock-like approach, since we need to evaluate two-body observables, and strictly speaking within DFT, one does not have access to the two-body densities.

### G. Principal Component Analysis

The parameters listed in Table II are highly correlated. To analyze these, we consider as significant changes  $\delta\chi_E \approx 0.1 \text{ MeV}$  since this is the typical level of sensitivity of the mass fits. We keep the changes relatively small because otherwise the model is not well approximated by a quadratic error model if  $\delta\chi_E > 0.1 \text{ MeV}$ . Numerically we find that even  $0.1 \text{ MeV}$  is too large, but yields qualitatively correct information after a full refitting. Note that  $\delta(\chi_E^2) = (\chi_E + \delta\chi_E)^2 - \chi_E^2 = 2\chi_E \delta\chi_E + (\delta\chi_E)^2$ , so we must normalize  $\delta(\chi_E^2)$  by  $2\chi_E \cdot 0.1 \text{ MeV}$  in order to consider changes  $\delta\chi_E \approx 0.1 \text{ MeV}$ .

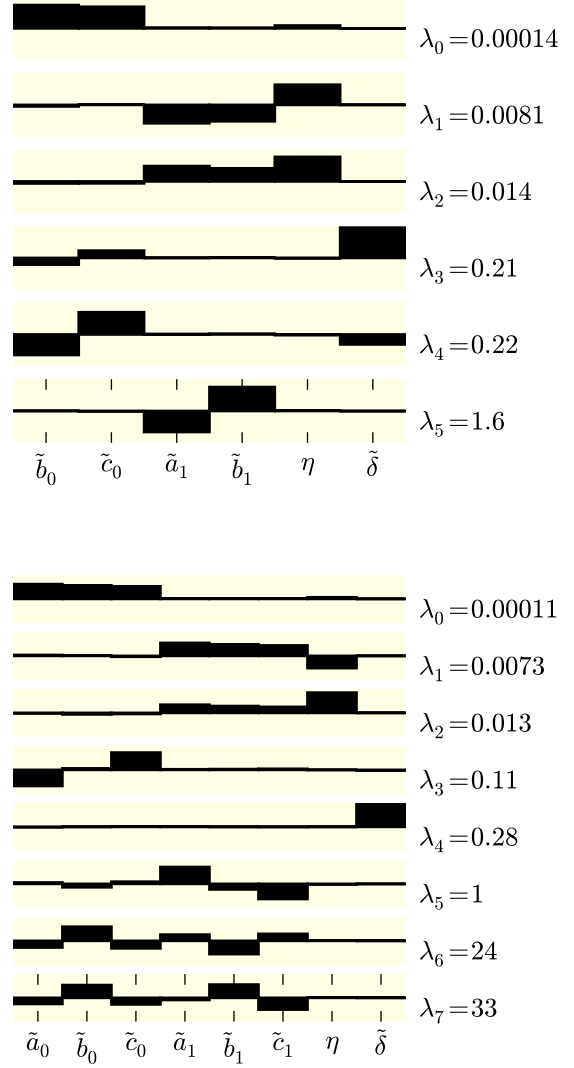


Figure 11 (Color online) Principal component analysis for the NEDF-1 fit (top) and the NEDF-3 fit (bottom). Plotted are the components of the eigenvectors  $\mathbf{v}_n$  defining the principal component Eq. (31b) as linear combinations of the various dimensionless parameters. From this we see that the most-significant component  $p_0 \approx \tilde{b}_0 + \tilde{c}_0$  which fixes the saturation energy to high precision. At the same time the component  $p_4 \approx (\tilde{b}_0 - \tilde{c}_0)$  in NEDF-1 (and similarly in NEDF-3n) is not well constrained. We also see that the least-significant component  $p_5 \approx \tilde{a}_1 - \tilde{b}_1$  is essentially unconstrained. For NEDF-3, we find three insensitive components, two of which can be used to set the smallest parameters  $a_0 = c_1 = 0$ . After removing these, one obtains a similar analysis as for NEDF-1 above.

To compare the parameters in a meaningful way, we must make them dimensionless and of order unity. We do this as in Table II by scaling with appropriate powers of  $\rho_* = 0.15 \text{ fm}^{-3}$  and  $\varepsilon_F = \frac{\hbar^2}{2m} (3\pi^2 \rho_*/2)^{2/3} = 35.29420 \text{ MeV}$ , which we take

as fixed parameters close to the saturation values:

$$\tilde{a}_j = \frac{a_j \rho_*^{2/3}}{\varepsilon_F}, \quad \tilde{b}_j = \frac{b_j \rho_*}{\varepsilon_F}, \quad \tilde{c}_j = \frac{a_j \rho_*^{4/3}}{\varepsilon_F}. \quad (30)$$

(It is important to retain a significant number of digits for isoscalar quantities, as it will be clearer below.) In particular, we consider the covariance matrix  $\mathbf{C}$  such that the residual deviation is

$$\frac{\delta(\chi_E^2)}{2\chi_E \cdot 0.1 \text{ MeV}} \approx \boldsymbol{\delta}^T \cdot \mathbf{C}^{-1} \cdot \boldsymbol{\delta} = \sum_n \frac{(\delta p_n)^2}{\lambda_n^2}. \quad (31a)$$

where  $\boldsymbol{\delta}$  is the deviations vector of the dimensionless parameters Eq. (30) from their best fit values as listed in Table II, and we have diagonalized  $\mathbf{C}\mathbf{v}_n = \lambda_n^2 \mathbf{v}_n$  to obtain the principal components  $p_n$

$$p_n = \mathbf{v}_n \cdot (\tilde{a}_0 \ \tilde{b}_0 \ \cdots \ \eta \ \tilde{\boldsymbol{\delta}}). \quad (31b)$$

Since the parameters are of order unity, we may directly consider the  $\lambda_n$  as a measure of the errors: changing  $p_n$  by  $\lambda_n$  will affect the fit on the scale of  $\delta\chi_E \approx 0.1 \text{ MeV}$ . Therefore, the smaller the value of the parameter  $\lambda_n$ , the more precisely the fit to nuclear masses constrains the value of the corresponding linear combination of NEDF parameters.

The principal components for fits NEDF-1 and NEDF-3 are shown in Fig. 11. Both show similar features that can be understood in terms of the saturation and symmetry parameters Eq. (18) which we may express as:

$$\frac{\varepsilon_0}{\varepsilon_F} = \frac{3}{5} + \tilde{a}_0 + \tilde{b}_0 + \tilde{c}_0, \quad (32a)$$

$$0 = \frac{3}{5} + \tilde{a}_0 + \frac{3}{2}\tilde{b}_0 + 2\tilde{c}_0, \quad (32b)$$

$$\frac{K}{-18\varepsilon_F} = \frac{3}{5} + \tilde{a}_0 - 2\tilde{c}_0, \quad (32c)$$

$$\frac{S}{\varepsilon_F} = \frac{3(2^{2/3}-1)}{5} + (\tilde{a}_1 + \tilde{b}_1 + \tilde{c}_1) + (\tilde{a}_2 + \tilde{b}_2 + \tilde{c}_2), \quad (32d)$$

$$\frac{L}{\varepsilon_F} = \frac{2S}{\varepsilon_F} + (\tilde{b}_1 + 2\tilde{c}_1) + (\tilde{b}_2 + 2\tilde{c}_2). \quad (32e)$$

The most significant component  $p_0$  in both fits is the sum of the  $j=0$  coefficients  $\tilde{a}_0 + \tilde{b}_0 + \tilde{c}_0$  which fixes the saturation energy  $\varepsilon_0$  Eq. (32a) to very high precision. Next are mixtures of  $\eta$  and the symmetry energy  $S$  Eq. (32d), which are correlated by the finite size of the nuclei; the latter is the sum of the  $j=1$  coefficients  $\tilde{a}_1 + \tilde{b}_1 + \tilde{c}_1$  (recall that these fits have no  $\beta^4$  components). Finally, we have some insignificant parameters, including  $\tilde{\boldsymbol{\delta}}$ .

In the case of NEDF-3, we see that two parameters are completely insignificant. These include  $\tilde{a}_0 \approx -0.088$  and  $\tilde{c}_1 = -0.017$ . These values are an order of magnitude smaller than the other coefficients: hence, the insignificant components can be easily removed by setting  $a_0 = c_1 = 0$  which we do in most of our fits.

Finally, both plots indicate that a combination of the  $j=1$  parameters is highly insignificant. Thus, in NEDF-1, the combination  $\tilde{b}_1 - \tilde{a}_1$  can be given almost any value of order unity without changing  $\chi_E$  more than 0.1 MeV. This is directly tested in NEDF-E, NEDF-Er, NEDF-En, and NEDF-Enr where we change the sign of  $b_1$ , setting  $a_1 = b_1 \rho_*^{2/3}$ . Indeed, we see that  $\chi_E$  changed by about 0.1 MeV. Notice from Table III that the slope of the symmetry energy  $L_2$  changes from about 30 MeV to 70 MeV while the other parameters remain about the same. This also significantly changes the neutron skin thickness, demonstrating a correlation between  $L_2$  and the skin thickness, similar to that seen in other mean-field models (Viñas *et al.*, 2014). This is consistent with Eq. (32e) where we see that  $\tilde{b}_1$  gives us a direct handle on  $L_2$ .

#### IV. DYNAMICAL PROPERTIES

The NEDF can be used to study a variety of dynamical phenomena, excitation of nuclei by various external probes and various (large amplitude) collective modes, low energy collisions of nuclei, induced fission and fusion, etc. A dynamical interpretation of the functional follows by considering a coupled hydrodynamic theory of protons and neutrons.

Consider first a single species with number density  $\rho$  and a local momentum potential  $\phi$  such that the local fluid momentum  $\mathbf{p} = m\mathbf{v} = \nabla\phi$ . The Euler-Lagrange equations for the following Lagrangian density

$$\mathcal{L} = -\rho \left( \phi + \frac{1}{2m} (\nabla\phi)^2 \right) - \mathcal{E}(\rho) - \eta \frac{\hbar^2}{2m} (\nabla\sqrt{\rho})^2 \quad (33a)$$

define the following hydrodynamic equations:

$$\dot{\rho} + \nabla \cdot (\rho\mathbf{v}) = 0, \quad (33b)$$

$$\dot{\phi} + \frac{mv^2}{2} + \mathcal{E}'(\rho) - \eta \frac{\hbar^2}{2m} \frac{\nabla^2 \sqrt{\rho}}{\sqrt{\rho}} = 0, \quad (33c)$$

the latter of which is sometimes expressed as

$$m\dot{\mathbf{v}} + \nabla \left[ \frac{mv^2}{2} + \mathcal{E}'(\rho) - \eta \frac{\hbar^2}{2m} \frac{\nabla^2 \sqrt{\rho}}{\sqrt{\rho}} \right] = 0. \quad (33d)$$

Recognizing that the last term in these equations has the form of a ‘‘quantum pressure’’ term with a modified Planck’s constant  $\tilde{\hbar} = \eta^{1/2} \hbar$ , one can check that this hydrodynamic theory is equivalent to the following ‘‘quantum’’ theory for a wavefunction  $\psi = \sqrt{\rho} \exp(i\phi/\tilde{\hbar}) = \sqrt{\rho} \exp(i\theta)$ :

$$\mathcal{L}(\psi, \dot{\psi}) = \psi^\dagger \left( i\tilde{\hbar} \partial_t + \frac{\tilde{\hbar}^2 \nabla^2}{2m} \right) \psi - \mathcal{E}(\rho), \quad (34a)$$

$$i\tilde{\hbar} \dot{\psi} = -\frac{\tilde{\hbar}^2}{2m} \nabla^2 \psi + \mathcal{E}'(\rho) \psi. \quad (34b)$$

Note that with these equations, the action is invariant under the Galilean boost to a frame with velocity  $\mathbf{v}$ :

$$\psi(\mathbf{x}, t) \rightarrow e^{i\theta} \psi(\mathbf{x} - \mathbf{v}t, t), \quad \tilde{\hbar}\theta = m\mathbf{v} \cdot \mathbf{x} - \frac{mv^2 t}{2}. \quad (35)$$



Equations (34) have exactly the same form as a non-linear Schrödinger equation that would be used to study the collective wavefunction of a superfluid Bose-Einstein condensate (BEC) with homogeneous energy density  $\mathcal{E}(\rho)$ . The implementation of the hydrodynamic equations as a non-linear Schrödinger equation allows for stable numerical implementations and may be solved efficiently using standard algorithms. Somewhat surprisingly this ‘‘Schrödinger equation’’ admits ‘‘quantized vortices’’, albeit with a modified ‘‘Planck’s constant’’  $\tilde{\hbar}$ . The quantization of vortices here is purely a formal artifact since it depends on the free parameter  $\eta$ . Although it might be appealing to consider Eqs. (34) as a theory for superfluid dimers comprising two protons or two neutrons, the best-fit value of  $\eta \approx 0.5$  does not presently admit this interpretation. As mentioned earlier, to restore properly quantized vortices requires  $\eta = 1/4$  and a rescaling of the wavefunction, by normalizing it to the total particle number – i.e.  $2\rho = |\psi|^2$  – so that the factors of  $\eta = 1/4$  cancel in Eqs. (34), yielding a properly normalized Schrödinger equation.

One can similarly recast our complete NEDF in terms of two ‘‘complex wavefunctions’’ with a modified ‘‘Planck’s constant’’  $\tilde{\hbar} = \sqrt{\eta}\hbar$ :

$$\psi_{n,p} = \sqrt{\rho_{n,p}} \exp(i\theta_{n,p}), \quad m_{n,p} \mathbf{v}_{n,p} = \tilde{\hbar} \nabla \theta_{n,p}, \quad (36a)$$

through the Lagrangian density

$$\mathcal{L} = i\tilde{\hbar}(\psi_n^\dagger \dot{\psi}_n + \psi_p^\dagger \dot{\psi}_p) - \mathcal{E}[\psi_n, \psi_p] \quad (36b)$$

where

$$\begin{aligned} \mathcal{E}[\psi_n, \psi_p] &= \frac{\tilde{\hbar}^2}{2m_n} \nabla \psi_n^\dagger \cdot \nabla \psi_n + \frac{\tilde{\hbar}^2}{2m_p} \nabla \psi_p^\dagger \cdot \nabla \psi_p + \\ &+ \mathcal{E}_{\text{entrain}}(\psi_n, \psi_p) + \mathcal{E}_h(\rho_n, \rho_p), \end{aligned} \quad (36c)$$

and the homogeneous energy-density (no gradients) is

$$\begin{aligned} \mathcal{E}_h(\rho_n, \rho_p) &= \frac{3\hbar^2(3\pi^2)^{2/3}}{10} \left( \frac{\rho_n^{5/3}}{m_n} + \frac{\rho_p^{5/3}}{m_p} \right) + \\ &+ \frac{1}{2} V_C \rho_c - \frac{e^2 \pi}{4} \left( \frac{3\rho_p}{\pi} \right)^{4/3} \\ &+ \sum_{j=0}^2 (a_j \rho^{5/3} + a_j \rho^{6/3} + a_j \rho^{7/3}) \left( \frac{\rho_n - \rho_p}{\rho} \right)^{2j} + \end{aligned} \quad (36d)$$

The representation of the densities in the form (36a) is similar in spirit to the decomposition of the single-particle density matrix championed in the theory of large amplitude collective motion  $\rho \rightarrow e^{-i\chi} \rho e^{i\chi}$  (Baranger and Vénéroni, 1978; Brink *et al.*, 1976; Ring and Schuck, 2004). The energy of a nucleus is thus also uniquely separated into the collective kinetic energy (the terms explicitly depending on  $\psi_{n,p}$ ) and the internal energy depends only on the ‘‘shape’’ of a nucleus, with no internal quasi-particle excitations.

Ignoring for a moment the entrainment term  $\mathcal{E}_{\text{entrain}}(\psi_n, \psi_p)$ , dynamics can be implemented using the following coupled non-linear ‘‘Schrödinger’’ equations:

$$i\tilde{\hbar} \frac{\partial \psi_{n,p}}{\partial t} = -\frac{\tilde{\hbar}^2}{2m_{n,p}} \nabla^2 \psi_{n,p} + U_{n,p} \psi_{n,p}, \quad (37a)$$

$$U_{n,p} = \frac{\partial \mathcal{E}_h(\rho_n, \rho_p)}{\partial \rho_{n,p}}. \quad (37b)$$

## A. Entrainment

As mentioned above, this theory is covariant under Galilean boosts to a frame with velocity  $\mathbf{v}$  (Eq. (35)). Since both protons and neutrons experience the same boost  $\mathbf{v}_{n,p} \rightarrow \mathbf{v}_{n,p} + \mathbf{v}$ , we can introduce an additional Galilean invariant term in the two-component system proportional to  $|\mathbf{v}_n - \mathbf{v}_p|^2$ , obtaining the collective kinetic energy:

$$\frac{m_n \rho_n v_n^2}{2} + \frac{m_p \rho_p v_p^2}{2} + \alpha \frac{m_n m_p \rho_n \rho_p |\mathbf{v}_n - \mathbf{v}_p|^2}{2m\rho}. \quad (38)$$

The parameter  $\alpha$  controls the entrainment of the neutron and proton fluids, and the form has been chosen so that the term vanishes when either density vanishes.

As with the quadratic terms above which enter the functional as  $|\nabla \psi_{n,p}|^2$ , the entrainment term must be constructed from the wavefunctions rather than from the velocities to avoid singularities when the density vanishes (i.e. in the cores of quantized vortices or in the tails of the nucleus). This can be done by noting that the following ‘‘currents’’ transform under Galilean boosts as

$$\mathbf{J}_{n,p} = -i\tilde{\hbar} \psi_{n,p}^\dagger \nabla \psi_{n,p}, \quad \mathbf{J}_{n,p} \rightarrow \mathbf{J}_{n,p} + m_{n,p} \rho_{n,p} \mathbf{v}. \quad (39)$$

Hence, we define the Galilean invariant entrainment term:

$$\begin{aligned} \mathcal{E}_{\text{entrain}}(\psi_n, \psi_p) &= \\ &= \alpha \frac{m_n m_p \rho_n \rho_p}{2m\rho_0} \left| \frac{\mathbf{J}_n}{m_n \rho_n} - \frac{\mathbf{J}_p}{m_p \rho_p} \right|^2 \\ &= \alpha \frac{\tilde{\hbar}^2}{2m\rho} \left| \frac{m_p^{1/2}}{m_n^{1/2}} \psi_p \nabla \psi_n - \frac{m_n^{1/2}}{m_p^{1/2}} \psi_n \nabla \psi_p \right|^2. \end{aligned} \quad (40)$$

For static properties, this term has the form

$$\begin{aligned} \mathcal{E}_{\text{entrain}}(\rho_n, \rho_p) &= \\ &= \alpha \frac{\tilde{\hbar}^2}{2m\rho} \left| \frac{m_p^{1/2}}{m_n^{1/2}} \rho_p^{1/2} \nabla \rho_n^{1/2} - \frac{m_n^{1/2}}{m_p^{1/2}} \rho_n^{1/2} \nabla \rho_p^{1/2} \right|^2, \end{aligned} \quad (41)$$

and leads to a coupling between the neutron and proton density gradients  $\nabla \rho_n \cdot \nabla \rho_p$ . Bodmer (1960) introduced this type of term, and it also appears in various Skyrme parameterizations of the NEDF. By varying  $\alpha$  from  $-0.5$  to  $0.5$ ,  $\chi_E$  changed by at most 15 keV. The significant effect of this term is seen

however in the dynamics, where the motion of one fluid will drag along the other, affecting strongly the excitation energies of isovector modes such as the GDRs.

Entrainment (the Andreev-Bashkin effect) was predicted by Andreev and Bashkin (1975) to occur in superfluid mixtures of  $^3\text{He}$  and  $^4\text{He}$ , and is rather surprising at first sight, since superfluids are expected to flow without resistance. In particular, one might have expected that if somehow one would bring into motion only one superfluid component, superfluidity will have the consequence that the other component remains at rest. The entrainment term (40) is indeed dissipationless, and thus it does not violate superfluidity, but allows the motion of one superfluid to influence (entrain) the other. It is natural to expect a similar phenomenon to arise in nuclei, where proton and neutron (super)fluids can coexist. Entrainment should also play a role in neutron stars and has been studied intermittently since 1975 (Alpar *et al.*, 1984; Babaev, 2004; Chamel, 2013; Chamel and Haensel, 2006; Gusakov and Haensel, 2005; Vardanyan and Sedrakyan, 1981; Volovik *et al.*, 1975). The formalism describing these systems is called three fluid hydrodynamics – two superfluids and one normal component – and is generalization of Landau’s two fluid hydrodynamic phenomenological model of superfluids at finite temperatures below, but the critical temperature. Since in nuclear systems both neutron and proton subsystems can have a superfluid and a normal components at finite temperatures, and since the normal components can move independently in isovector modes, a proper generalization of the superfluid dynamics to nuclear systems would be a four fluid hydrodynamics, with two superfluid and two normal components, thus a somewhat more complex system than the superfluid mixtures considered so far in literature.

## B. Shell Effects

Shell-corrections have a typical amplitude of several MeVs. Even though they represent a relatively small correction to the total energy of the system, they can have a major effect on low energy nuclear dynamics. Their magnitude is controlled by the spin-orbit interaction, the pairing effects, and the nuclear shape. There are several prescriptions one can use to compute shell corrections, but the idea behind them is the same. The shell-corrections are a function  $E_{\text{sc}}(\{\epsilon_k\})$  of single-particle energies  $\epsilon_k$

$$\mathbf{h}_\tau \psi_{\tau,k} = \epsilon_{\tau,k} \psi_{\tau,k}, \quad (42)$$

where  $\psi_{\tau,k}$  are the single-particle wave functions for the single-particle Hamiltonian  $\mathbf{h}_\tau$  for proton and neutrons  $\tau = n, p$ . This Hamiltonian is the functional derivative of the energy density

(here  $\alpha = 0$ )

$$\begin{aligned} \mathcal{F}[\rho_n, \rho_p] = & \sum_{k, \tau=n,p} \frac{\hbar^2}{2m_\tau} |\nabla \psi_{\tau,k}|^2 \\ & + \sum_{\tau=n,p} \left( \eta - \frac{1}{9} \right) \frac{\hbar^2}{2m_\tau} |\nabla \rho_\tau^{1/2}|^2 \\ & + \sum_{j=0}^2 \mathcal{E}_j(\rho) \beta^{2j} + \mathcal{E}_C(\rho_n, \rho_p) \\ & + \text{spin-orbit} + \text{pairing contributions}. \end{aligned} \quad (43)$$

The main difference between this energy density and Eq. (8) is that now the  $\psi_{\tau,k}$  are the single-particle neutron and proton wave functions.

There is an ambiguity in separating the contribution of the gradient terms and other forms of this energy density can be considered. For example, one can introduce an additional parameter  $\xi$  (which might have a density and even an isospin dependence) and define the energy density  $\mathcal{F}[\rho_n, \rho_p]$  as:

$$\begin{aligned} \mathcal{F}[\rho_n, \rho_p] = & \sum_{k, \tau=n,p} (1 + \xi) \frac{\hbar^2}{2m_\tau} |\nabla \psi_{\tau,k}|^2 \\ & - \xi \sum_{\tau=n,p} \frac{\hbar^2}{2m_\tau} \frac{3}{5} (3\pi^2)^{2/3} \rho_\tau^{5/3} \\ & + \sum_{\tau=n,p} \left( \eta - (1 + \xi) \frac{1}{9} \right) \frac{\hbar^2}{2m_\tau} |\nabla \rho_\tau^{1/2}|^2 \\ & + \sum_{j=0}^2 \mathcal{E}_j(\rho) \beta^{2j} + \mathcal{E}_C(\rho_n, \rho_p) \\ & + \text{spin-orbit} + \text{pairing contributions}. \end{aligned} \quad (44)$$

The introduction of such a parameter  $\xi$  requires adding additional terms to restore the Galilean invariance of this energy density functional (Engel *et al.*, 1975) (strictly speaking the Galilean invariance of the intrinsic energy of a nucleus), and its introduction will also lead to a modification of the Thomas-Reiche-Kuhn sum rule for GDR. The semiclassical limit of both Eqs. (43) and (44) are identical by construction.

As in the case of the unitary Fermi gas (Bulgac, 2007, 2013; Bulgac *et al.*, 2012a), without additional information from either the spectral weight function or from spectroscopy, the interpretation of the terms  $a_j \rho^{5/3}$  as either being the semiclassical limit of the appropriate kinetic energy densities or of interaction energy densities is ambiguous. This ambiguity is related to the discussion above.

The equations of motion (37a) have to be augmented now with the contribution to the potential arising from  $E_{\text{sc}}(\{\epsilon_k\})$  as follows:

$$\begin{aligned} i\tilde{\hbar} \frac{\partial \psi_{n,p}}{\partial t} = & - \frac{\tilde{\hbar}^2}{2m_{n,p}} \nabla^2 \psi_{n,p} + U_{n,p} \psi_{n,p} \\ & + \sum_l \frac{\partial E_{\text{sc}}(\{\epsilon_k\})}{\partial \epsilon_l} \frac{\delta \epsilon_l}{\delta \rho_{n,p}} \psi_{n,p}. \end{aligned} \quad (45)$$

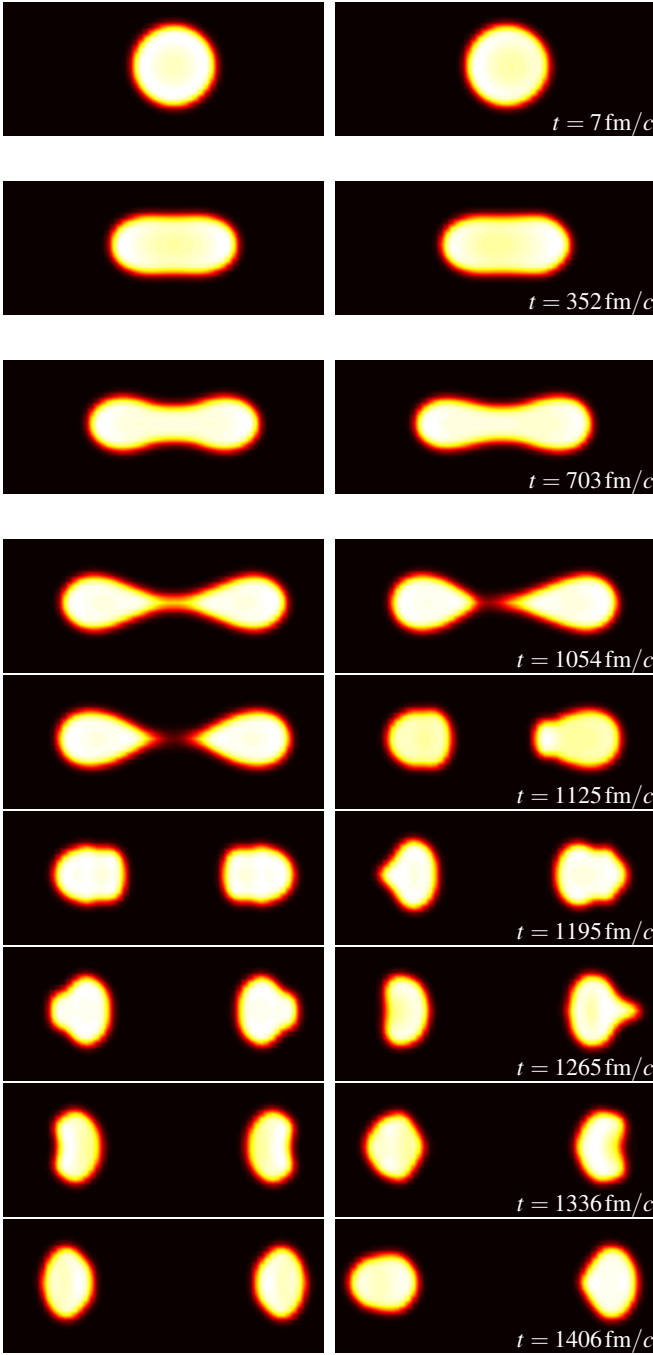


Figure 12 (Color online) Induced fission of  $^{238}\text{U}$  excited with an initial quadrupole and octupole potential velocity  $\theta_n(\mathbf{r}) = \theta_p(\mathbf{r}) = q_2(2z^2 - x^2 - y^2) + q_3(5z^2 - 3)z$  starting from the ground state, see Eqs. (36a). The symmetric case (left) has  $q_3 = 0$  and an excitation energy of 7.68 MeV (initial collective kinetic energy). The asymmetric case (right) has an excitation energy of 10.33 MeV (initial collective kinetic energy) and the final charges, neutron numbers, and atomic masses of the two fragments are  $Z_1 = 49.3$ ,  $N_1 = 78.4$ ,  $A_1 = 127.7$ ,  $Z_2 = 42.7$ ,  $N_2 = 67.6$ , and  $A_2 = 110.3$ . Both fragments emerge with a significant amount of collective excitation energy and several excited multipolarities. (Note that the interval between the first three frames is about 5 times the interval between the lower frames.)

The dynamics described by Eqs. (45) is in spirit similar to the constrained density TDHF approach developed by Oberacker and Umar (2015) and Umar and Oberacker (2006). The nuclear systems will evolve in time, while only the collective degrees of freedom are active, in exactly the same manner as the theory of Adiabatic TDHF (ATDHF) was envisioned (Baranger and Vénéroni, 1978; Brink *et al.*, 1976; Ring and Schuck, 2004). The present approach is formulated directly in terms of (all) relevant collective degrees of freedom and there is no difficulty in separating the degrees of freedom into intrinsic and collective. The definition of the collective degrees of freedom and their proper separation from the intrinsic ones is a problem practically unsurmountable in the usual theory of LACM (Dang *et al.*, 2000). The dynamics described by Eqs. (45), or their simplified form Eqs. (12a), is by default isentropic. There is no need and no difficulty in constructing either the inertia tensor or the potential energy surface, as the system naturally evolves from one point to another in the collective phase space.

### C. Induced Symmetric and Asymmetric Fission

In Fig. 12 we show the evolution of a  $^{238}\text{U}$  nucleus starting from the ground state with two different initial isoscalar velocity kicks and no shell-corrections, leading to symmetric and asymmetric fission respectively. The fragments emerge with a significant excitation energy and deformation, clearly not in the corresponding ground states. The excitation energy of the nucleus has two components, the collective flow given by Eq. (38) and the deformation and Coulomb energies given by Eq. (8) respectively. The total energy is naturally conserved. The results presented in these figures have been obtained by solving the full three-dimensional (3D) time-dependent equations (34), on a  $64^3$  spatial lattice. This takes about 30 minutes on a MacBook Pro using a MATLAB program about 250 line long (including the generation of the ground state and of the movie and related graphics).

### D. Giant Isovector Resonances

Equations (34) have also been used to extract the behavior of the GDRs as a function of the atomic mass  $A$ . As a function of the atomic mass, the NEDFs without entrainment yield  $\hbar\omega_{\text{GDR}} \approx 65 \dots 70/A^{1/3}$  MeV, which is too low (Piotr Magierski, private communication). Even though the entrainment term plays a small role when computing the ground state energies, it plays an important role in determining the excitation energies of isovector modes.

Let us consider for simplicity a nucleus with  $N = Z$ , in which we will neglect the Coulomb effects and the neutron-proton mass difference  $m \approx m_n \approx m_p$ . In this case in the ground state  $\rho_n(\mathbf{r}) \equiv \rho_p(\mathbf{r}) = \rho_0(\mathbf{r})/2 = |\psi_0(\mathbf{r})|^2$  and the density are determined from the nonlinear equation

$$-\frac{\hbar^2}{2m_\tau} \nabla^2 \psi_0 + \mathcal{E}'_0(\rho_0) \psi_0 = \mu_0 \psi_0. \quad (46)$$

Considering small amplitude isovector modes  $\rho_{n,p}(\mathbf{r}, t) = |\psi_0(\mathbf{r}) \pm \psi_1(\mathbf{r}, t)|^2$ , where  $\psi_0(\mathbf{r}) = \psi_0^*(\mathbf{r})$ , one can derive the equation:

$$i\hbar\dot{\psi}_1 = -(\eta + \alpha)\frac{\hbar^2}{2m}\nabla^2\psi_1 + 2\mathcal{E}'_0(\rho_0)\psi_1 + 8\frac{\mathcal{E}_1(\rho_0)}{\rho_0}(\psi_1 + \psi_1^*) - \alpha\frac{\hbar^2}{m}\psi_0\nabla\cdot\left(\frac{\nabla(\psi_0\psi_1)}{\psi_0^2}\right). \quad (47)$$

For  $\alpha > 0$  the effective mass is lowered (first term) and the stiffness increased (last term), which results in an increased value of the  $\hbar\omega_{\text{GDR}}$ . Thus, the entrainment term through the parameter  $\alpha$  provides a direct handle on isovector dynamics without significantly impacting the static properties of the NEDFs. One last remark: Eqs. (34) will only provide a good description of the collective modes and their corresponding transition strengths.

## V. CONCLUSIONS

The nuclear energy density functional (NEDF) developed in this work contains at most 7 significant parameters, each clearly related to specific properties of nuclei. In particular, to globally fit the measured ground state energies of 2375 nuclei, functionals NEDF-En and NEDF-Enr can achieve an rms residual of  $\chi_E \approx 2.6$  MeV to 2.7 MeV *with only 4 significant fit parameters* (and an insignificant pairing parameter  $\delta$ ).

Therefore NEDF-En and NEDF-Enr reproduce the behavior of the best nuclear mass formula, with fewer free parameters, and yet have many advantages; unlike nuclear mass formulas, these NEDFs also model the neutron and proton densities in the nuclei, allowing one to extract the charge radii. Fitting the masses alone gives an rms residual of  $\chi_r = 0.13$  fm for the corresponding 883 measured charge radii, while including them in the fit improves this to  $\chi_r = 0.05$  fm without significantly affecting the quality of the mass fits.

As in the mass formulas Eqs. (1) and (2), one needs two parameters  $b_0$  and  $c_0$ , which control the isoscalar nuclear properties and thus are needed to reproduce the symmetric nuclear binding energy and density. The isoscalar nuclear compressibility acquires a very reasonable value too, although the saturation density is a little low, but not well constrained by the mass fits alone.

Two other parameters  $a_1$  and  $b_1$  control the symmetry properties of nuclear matter, and are correlated with a gradient term with parameter  $\eta$  that controls the diffuseness of the nuclear surface. These are similar to the parameters  $a_I$  and  $a'_I$  in nuclear mass formula Eq. (2), but we find that the linear combination  $a_1 - b_1\rho_0^{1/3}$  is poorly constrained by the masses. This gives one an essentially independent control of the ‘‘local’’ symmetry energy slope  $L_2$  (not the full  $L$ , which is fully determined by the neutron equation of state), along with neutron skin thicknesses.

The addition of quartic isovector coefficients  $\beta^4$  permits the NEDF to match the neutron matter equation of state without significantly affecting the global mass fit. We thus find that the

masses and the neutron matter equation of state are essentially uncoupled.

These NEDF are suitable to study complex collective motion such nuclear fission, low energy collision of nuclei, their fusion, interactions with various external time-dependent probes, structure and dynamics of the neutron star crust, nucleosynthesis, etc. in a computationally efficient manner in order to better gain intuition and understanding about nuclear dynamics. Finally, an entrainment term with parameter  $\alpha$  controls the energies of the isovector nuclear excitation modes and together with an additional parameter  $\xi$  one can control the value of the Thomas-Reiche-Kuhn sum rule.

This NEDF contains several new elements with respect to commonly used Skyrme-like density functional theories:

- Terms proportional to  $\rho^{5/3}$ , similar to those found in the study of the unitary Fermi gas.
- The gradient terms in Eq. (8) proportional to  $\eta|\nabla\rho_\tau^{1/2}|^2 = \eta|\nabla\rho_\tau|^2/4\rho_\tau$  or to  $\alpha\nabla\rho_n^{1/2}\cdot\nabla\rho_p^{1/2}$ .
- There is a need to consider quartic terms in isospin density  $(\rho_n - \rho_p)^4$  in the NEDF if one aims to describe correctly both nuclei and neutron matter within the same unified framework, and in particular the neutron star crust. The binding energies, charge radii, and neutron skin thickness appear to be insensitive to the properties of the neutron equation of state, which can essentially be fit independently. The position of the neutron dripline appears to be controlled by the full symmetry energy  $S$  and its density dependence  $L$ , unlike neutron skin thickness, which is controlled by the ‘‘local’’ density dependence of the symmetry energy  $L_2$ . The properties of nuclear matter in stellar environments (when  $N \gg Z$ ) will therefore be controlled by  $S$  and  $L$ , influencing for example the reaction flow in the r-process, the structure of the neutron star crust, and the vortex pinning mechanism in neutron star crust.
- Entrainment terms  $\alpha\mathbf{v}_n \cdot \mathbf{v}_p$  do not appear in any standard theory of large amplitude collective motion in nuclear physics (Baranger and Vénérone, 1978; Brink *et al.*, 1976; Ring and Schuck, 2004), despite being allowed by symmetry. They have direct analogues in superfluid mixtures – the Andreev-Bashkin effect – and are as natural to consider in the presence of mixed proton and neutron superfluids in neutron stars as they are in mixtures of  $^3\text{He}$  and  $^4\text{He}$  superfluids (Andreev and Bashkin, 1975; Vardanyan and Sedrakyan, 1981; Volovik *et al.*, 1975). These terms have little influence of the ground state binding energies, but a strong effect on excited isovector modes and such terms have been discussed in the physics of neutron stars and determined to be relevant for the description of glitches (Alpar *et al.*, 1984; Babaev, 2004; Chamel, 2013; Chamel and Haensel, 2006; Gusakov and Haensel, 2005).

To extend the accuracy of this NEDF to reproduce finer details of nuclear binding energies (screening of the Coulomb interaction and a correct treatment of the exchange term, isospin and charge symmetry breaking effects, Wigner energy, effects due to the restoration of various other broken symmetries, etc.) first requires an accurate accounting of shell effects; the procedure is outlined. Next, the parameters  $\alpha$  and  $\xi$  can be determined by fixing the correct value of the Thomas-Reiche-Kuhn sum rule. Additional parameters should be introduced into the NEDF to model the appropriate physics such as spin-orbit interactions and pairing. The NEDF model is physically intuitive, providing a framework for systematically adding physically motivated parameters.

The ability to study dynamical phenomena is a great advantage of the present approach. It is not difficult to develop a generalization of the NEDF to finite temperatures and to include dissipation in the dynamics. In particular it would be extremely interesting to establish the general trends in which mass and charge asymmetry influences the excitation energies and average angular momentum of fragments in induced fission as a function of the initial energy injected into the nucleus and impact parameters in case of reactions. It would be interesting as well to study the sticking probability of two colliding heavy-ions as a function of the mass and charge ratio, impact parameter and relative velocity.

A great advantage of the present approach is to provide a clear strategy for improving the quality of NEDFs by separating the various energy scales. Here we have identified the bulk properties, and shown that they can be properly accounted for with a minimal number of parameters. Now we have a clear path forward to refine the structure of the NEDF to properly account for smaller corrections. In this respect the approach outlined here is similar in spirit to an effective field theory. The next step is to introduce the spin-orbit coupling, the pairing coupling constants (about which there is already an abundance of information), and to pinpoint the values of the couplings  $\alpha$  and  $\xi$ , all of which have a very small effect on the nuclear bulk properties. The major impact of these new constants will be on the shell-correction energies, and extensive past experience indicates that the rms energy should be reduced drastically from about 2.6 MeV to close to 0.5 MeV or so (Bohr and Mottelson, 1998; Brack *et al.*, 1972, 1985; Moller *et al.*, 1995; Möller *et al.*, 2012; Myers and Swiatecki, 1974, 1990, 1991, 1996, 1969, 1966; Ring and Schuck, 2004; Strutinsky, 1966, 1967, 1968; Strutinsky and Magner, 1976) or even below, at which point quantum chaos will likely need to be properly accounted for (Åberg, 2002; Barea *et al.*, 2005; Bohigas and Leboeuf, 2002a,b; Hirsch *et al.*, 2005, 2004; Molinari and Weidenmüller, 2006, 2004; Olofsson *et al.*, 2006, 2008).

## ACKNOWLEDGMENTS

We are grateful to George F. Bertsch for numerous discussions and suggestions, to Sanjay Reddy and David B. Kaplan, who urged us to explore the role of  $\nabla\rho_n \cdot \nabla\rho_p$  types of terms,

to Rebecca Surman for discussions about aspects of neutron star physics, and to Jeremy W. Holt for valuable comments. This work was supported in part by US DOE Grant No. DE-FG02-97ER-41014. Some calculations reported here have been performed at the University of Washington Hyak cluster funded by the NSF MRI Grant No. PHY-0922770.

## VI. SUPPLEMENTAL MATERIAL

Tables with the results of the numerical fits of various NEDFs presented in Table II, along with the Python code used to perform these fits and a MATLAB code used to determine the ground state and the 3D time-dependent fission process illustrated in Fig 12 can be downloaded from <http://faculty.washington.edu/bulgac/NEDF>.

## REFERENCES

- Abe, T. and R. Seki (2009a), “From low-density neutron matter to the unitary limit,” *Phys. Rev. C* **79**, 054003.
- Abe, T. and R. Seki (2009b), “Lattice calculation of thermal properties of low-density neutron matter with pionless  $NN$  effective field theory,” *Phys. Rev. C* **79**, 054002.
- Åberg, Sven (2002), “Nuclear physics: Weighing up nuclear masses,” *Nature* **417** (6888), 499–501.
- Adelberger, E G, A. García, R. G. Hamish Robertson, K. A. Snover, A. B. Balantekin, K. Heeger, M. J. Ramsey-Musolf, D. Bemmerer, A. Junghans, C. A. Bertulani, J.-W. Chen, H. Costantini, P. Prati, M. Couder, E. Uberseder, M. Wiescher, R. Cyburt, B. Davids, S. J. Freedman, M. Gai, D. Gazit, L. Gialanella, G. Imbriani, U. Greife, M. Hass, W. C. Haxton, T. Itahashi, K. Kubodera, K. Langanke, D. Leitner, M. Leitner, P. Vetter, L. Winslow, L. E. Marcucci, T. Motobayashi, A. Mukhamedzhanov, R. E. Tribble, Kenneth M. Nollett, F. M. Nunes, T.-S. Park, P. D. Parker, R. Schiavilla, E. C. Simpson, C. Spitaleri, F. Strieder, H.-P. Trautvetter, K. Suemmerer, and S. Typel (2011), “Solar fusion cross sections. II. the  $pp$  chain and CNO cycles,” *Rev. Mod. Phys.* **83**, 195–245.
- Afanasjev, A V, M. Beard, A. I. Chugunov, M. Wiescher, and D. G. Yakovlev (2012), “Large collection of astrophysical  $S$  factors and their compact representation,” *Phys. Rev. C* **85**, 054615.
- Agbemava, S E, A. V. Afanasjev, D. Ray, and P. Ring (2014), “Global performance of covariant energy density functionals: Ground state observables of even-even nuclei and the estimate of theoretical uncertainties,” *Phys. Rev. C* **89**, 054320.
- Alpar, M A, S. A. Langer, and J. A. Sauls (1984), “Rapid postglitch spin-up of the superfluid core in pulsars,” *Astrophys. J.* **282**, 533.
- Andreev, A F, and E. P. Bashkin (1975), “3-velocity hydrodynamics of superfluid solutions,” *Sov. Phys.-JETP* **42**, 164, *zh. Éksp. Teor. Fiz.* **69**, 319 (1975).
- Angeli, I, and K.P. Marinova (2013), “Table of experimental nuclear ground state charge radii: An update,” *At. Data. Nucl. Data Tables* **99** (1), 69 – 95.
- Aston, F W (1920), “Isotopes and atomic weights,” *Nature* **105** (2646), 605 – 636.
- Audi, G, M. Wang, A.H. Wapstra, F.G. Kondev, M. MacCormick, X. Xu, and B. Pfeiffer (2012), “The ame2012 atomic mass evaluation,” *Chinese Phys. C* **36** (12), 1287.
- Avogadro, P, F. Barranco, R. A. Brogna, and E. Vigezzi (2007), “Quantum calculation of vortices in the inner crust of neutron stars,” *Phys. Rev. C* **75** (1), 012805.

- Avogadro, P, F. Barranco, R. A. Broglia, and E. Vigezzi (2008), “Vortex-nucleus interaction in the inner crust of neutron stars,” *Nucl. Phys. A* **811** (3–4), 378–412.
- Babaev, Egor (2004), “Andreev-Bashkin effect and knot solitons in an interacting mixture of a charged and a neutral superfluid with possible relevance for neutron stars,” *Phys. Rev. D* **70**, 043001.
- Baker, Jr, George A (1999), “Neutron matter model,” *Phys. Rev. C* **60** (5), 054311.
- Baldo, M, L. M. Robledo, P. Schuck, and X. Viñas (2013), “New Kohn-Sham density functional based on microscopic nuclear and neutron matter equations of state,” *Phys. Rev. C* **87**, 064305.
- Baldo, M, P. Schuck, and X. Viñas (2008), “Kohn–Sham density functional inspired approach to nuclear binding,” *Phys. Lett. B* **663** (5), 390–394.
- Balian, R, and C Bloch (1970), “Distribution of eigenfrequencies for the wave equation in a finite domain: I. Three-dimensional problem with smooth boundary surface,” *Ann. Phys. (NY)* **60** (2), 401–447.
- Balian, R, and C. Bloch (1971), “Distribution of eigenfrequencies for the wave equation in a finite domain. II. Electromagnetic field. Riemannian spaces,” *Ann. Phys. (NY)* **64** (1), 271–307.
- Balian, R, and C. Bloch (1972), “Distribution of eigenfrequencies for the wave equation in a finite domain: III. Eigenfrequency density oscillations,” *Ann. Phys. (NY)* **69** (1), 76–160.
- Baltes, Heinrich P, and Eberhard R. Hilf (1976), *Spectra of finite systems* (Bibliographisches Institut, Mannheim).
- Baranger, M, and M. Vénéroni (1978), “An adiabatic time-dependent Hartree-Fock theory of collective motion in finite systems,” *Ann. Phys. (NY)* **114** (1-2), 123–200.
- Barea, José, Alejandro Frank, Jorge G. Hirsch., and Piet Van Isacker (2005), “Nuclear masses set bounds on quantum chaos,” *Phys. Rev. Lett.* **94** (10), 102501.
- Baym, Gordon, Hans A. Bethe, and Christopher J Pethick (1971), “Neutron star matter,” *Nucl. Phys. A* **175** (2), 225–271.
- Bender, Michael, Paul-Henri Heenen, and Paul-Gerhard Reinhard (2003), “Self-consistent mean-field models for nuclear structure,” *Rev. Mod. Phys.* **75** (1), 121–180.
- Bethe, H A, and R. F. Bacher (1936), “Nuclear Physics A. Stationary states of nuclei,” *Rev. Mod. Phys.* **8** (2), 82–229.
- Bodmer, A R (1960), “Neutron and proton densities in nuclei and the semi-empirical mass formula,” *Nucl. Phys.* **17** (0), 388–420.
- Bohigas, O, and P. Leboeuf (2002a), “Erratum: Nuclear masses: Evidence of order-chaos coexistence [Phys. Rev. Lett. 88, 092502 (2002)],” *Phys. Rev. Lett.* **88** (12), 129903.
- Bohigas, O, and P. Leboeuf (2002b), “Nuclear masses: Evidence of order-chaos coexistence,” *Phys. Rev. Lett.* **88** (9), 092502.
- Bohigas, O, S. Tomsovic, and D. Ullmo (1993), “Manifestations of classical phase space structures in quantum mechanics,” *Phys. Rep.* **223** (2), 43–133.
- Bohr, Aage, and Ben R. Mottelson (1998), *Nuclear Structure* (World Scientific, Singapore).
- Bordag, M, and I. Pirozhenko (2010), “Vacuum energy between a sphere and a plane at finite temperature,” *Phys. Rev. D* **81**, 085023.
- Brack, M, Jens Damgaard, A. S. Jensen, H. C. Pauli, V. M. Strutinsky, and C. Y. Wong (1972), “Funny hills: The shell-correction approach to nuclear shell effects and its applications to the fission process,” *Rev. Mod. Phys.* **44** (2), 320–405.
- Brack, M, C Guet, and H. B Håkansson (1985), “Selfconsistent semiclassical description of average nuclear properties—a link between microscopic and macroscopic models,” *Phys. Rep.* **123** (5), 275–364.
- Brack, M, B.K. Jennings, and Y.H. Chu (1976), “On the extended Thomas-Fermi approximation to the kinetic energy density,” *Phys. Lett. B* **65** (1), 1–4.
- Brack, Matthias (1993), “The physics of simple metal clusters: self-consistent jellium model and semiclassical approaches,” *Rev. Mod. Phys.* **65** (3), 677–732.
- Brack, Matthias, and Rajat K Bhaduri (1997), *Semiclassical physics*, *Frontiers in physics*, Vol. 96 (Addison-Wesley, Advanced Book Program, Reading, Mass.).
- Brink, D M, M. J. Giannoni, and M. Veneroni (1976), “Derivation of an adiabatic time-dependent Hartree-Fock formalism from a variational principle,” *Nucl. Phys. A* **258** (2), 237–256.
- Brown, B Alex (2013), “Constraints on the Skyrme equations of state from properties of doubly magic nuclei,” *Phys. Rev. Lett.* **111** (23), 232502.
- Brown, B Alex, and A. Schwenk (2014), “Constraints on Skyrme equations of state from properties of doubly magic nuclei and *ab initio* calculations of low-density neutron matter,” *Phys. Rev. C* **89** (1), 011307.
- Bulgac, Aurel (1988), “Semilocal approach to nonlocal equations,” *Nucl. Phys. A* **487** (2), 251–268.
- Bulgac, Aurel (2002), “Local Density Approximation for Systems with Pairing Correlations,” *Phys. Rev. C* **65**, 051305(R).
- Bulgac, Aurel (2007), “Local density functional theory for superfluid fermionic systems: The unitary gas,” *Phys. Rev. A* **76**, 040502.
- Bulgac, Aurel (2013), “Time-dependent density functional theory and the real-time dynamics of Fermi superfluids,” *Annu. Rev. Nucl. Part. Sci.* **63**, 97–121.
- Bulgac, Aurel, Michael McNeil Forbes, Michelle M. Kelley, Kenneth J. Roche, and Gabriel Wlazłowski (2014), “Quantized Superfluid Vortex Rings in the Unitary Fermi Gas,” *Phys. Rev. Lett.* **112**, 025301.
- Bulgac, Aurel, Michael McNeil Forbes, and Piotr Magierski (2012a), “The Unitary Fermi Gas: From Monte Carlo to Density Functionals,” Chap. 9, vol. 836 of (Zwenger, 2012), pp. 305–373.
- Bulgac, Aurel, Michael McNeil Forbes, and Rishi Sharma (2013), “Strength of the vortex-pinning interaction from real-time dynamics,” *Phys. Rev. Lett.* **110** (13), 241102.
- Bulgac, Aurel, and Caio Lewenkopf (1993), “Stable deformations in large metallic clusters,” *Phys. Rev. Lett.* **71** (25), 4130–4133.
- Bulgac, Aurel, Yuan-Lung Luo, Piotr Magierski, Kenneth J. Roche, and Yongle Yu (2011), “Real-time dynamics of quantized vortices in a unitary Fermi superfluid,” *Science* **332** (6035), 1288–1291.
- Bulgac, Aurel, Yuan-Lung Luo, and Kenneth J. Roche (2012b), “Quantum Shock Waves and Domain Walls in the Real-Time Dynamics of a Superfluid Unitary Fermi Gas,” *Phys. Rev. Lett.* **108** (15), 150401.
- Bulgac, Aurel, and Piotr Magierski (2001), “Quantum corrections to the ground state energy of inhomogeneous neutron matter,” *Nucl. Phys. A* **683** (1–4), 695–712.
- Bulgac, Aurel, and Piotr Magierski (2002), “Erratum to: “Quantum corrections to the ground state energy of inhomogeneous neutron matter,”,” *Nucl. Phys. A* **703** (3–4), 892–.
- Bulgac, Aurel, Piotr Magierski, and A. Wirzba (2005), “Fermionic Casimir effect in case of Andreev reflection,” *Europhys. Lett.* **72** (3), 327–333.
- Bulgac, Aurel, Piotr Magierski, and Andreas Wirzba (2006), “Scalar Casimir effect between Dirichlet spheres or a plate and a sphere,” *Phys. Rev. D* **73**, 025007.
- Bulgac, Aurel, and Vasily R. Shaginyan (1996), “A systematic surface contribution to the ground-state binding energies,” *Nucl. Phys. A* **601** (1), 103–116.
- Bulgac, Aurel, and Sukjin Yoon (2009), “Large amplitude dynamics of the pairing correlations in a unitary Fermi gas,” *Phys. Rev. Lett.* **102** (8), 085302.
- Bulgac, Aurel, and Yongle Yu (2002), “Renormalization of the Hartree-Fock-Bogoliubov equations in the case of a zero range

- pairing interaction,” *Phys. Rev. Lett.* **88** (4), 042504.
- Bulgac, Aurel, and Yongle Yu (2003), “Vortex state in a strongly coupled dilute atomic fermionic superfluid,” *Phys. Rev. Lett.* **91** (19), 190404.
- Canaguier-Durand, Antoine, Paulo A. Maia Neto, Astrid Lambrecht, and Serge Reynaud (2010), “Thermal Casimir effect for Drude metals in the plane-sphere geometry,” *Phys. Rev. A* **82**, 012511.
- Carlson, J., and Sanjay Reddy (2005), “Asymmetric two-component fermion systems in strong coupling,” *Phys. Rev. Lett.* **95**, 060401.
- Casimir, H B G (1948), “On the attraction between two perfectly conducting plates,” *Proc. K. Ned. Akad. Wet.* **51**, 793.
- Chamel, N (2013), “Crustal entrainment and pulsar glitches,” *Phys. Rev. Lett.* **110**, 011101.
- Chamel, Nicolas, and Pawel Haensel (2006), “Entrainment parameters in a cold superfluid neutron star core,” *Phys. Rev. C* **73**, 045802.
- Dang, Giu Do, Abraham Klein, and Niels R. Walet (2000), “Self-consistent theory of large-amplitude collective motion: applications to approximate quantization of nonseparable systems and to nuclear physics,” *Phys. Rep.* **335** (3-5), 93 – 274.
- De Vries, H. C. W. De Jager, and C. De Vries (1987), “Nuclear charge-density-distribution parameters from elastic electron scattering,” *At. Data. Nucl. Data Tables* **36**, 495 – 536.
- Delaroche, J P, M. Girod, J. Libert, H. Goutte, S. Hilaire, S. Péru, N. Pillet, and G. F. Bertsch (2010), “Structure of even-even nuclei using a mapped collective hamiltonian and the d1s gogny interaction,” *Phys. Rev. C* **81**, 014303.
- Dreizler, Reiner M, and Eberhard K. U. Gross (1990), *Density Functional Theory: An Approach to the Quantum Many-Body Problem* (Springer-Verlag, Berlin).
- Eddington, A S (1920), “The internal constitution of the stars,” *Nature* **106** (2653), 14–20.
- Engel, Y M, D. M. Brink, K. Goeke, S. J. Krieger, and D. Vautherin (1975), “Time-dependent Hartree-Fock theory with Skyrme’s interaction,” *Nucl. Phys. A* **249** (2), 215 – 238.
- Erler, J, N. Birge, M. Kortelainen, W. Nazarewicz, E. Olsen, A. M. Perhac, and M. Stoitsov (2012), “The limits of the nuclear landscape,” *Nature* **486**, 509–512.
- Erler, J, C. J. Horowitz, W. Nazarewicz, M. Rafalski, and P-G. Reinhard (2013), “Energy density functional for nuclei and neutron stars,” *Phys. Rev. C* **87**, 044320.
- Fantina, A F, N. Chamel, J. M. Pearson, and S. Goriely (2014), “Constraints on the equation of state of cold dense matter from nuclear physics and astrophysics,” *EPJ Web Conf.* **66**, 07005.
- Fayans, S A (1998), “Towards a universal nuclear density functional,” *JETP Lett.* **68** (3), 169–174.
- Fisher, M E, and P. G. de Gennes (1978), “Phénomènes aux parois dans un mélange binaire critique,” *C. R. Acad. Sci. Ser. B* **287**, 207.
- Gandolfi, S, A. Gezerlis, and J. Carlson (2015), “Neutron matter from low to high density,” arXiv:1501.0567.
- Gasques, L R, A. V. Afanasjev, E. F. Aguilera, M. Beard, L. C. Chamon, P. Ring, M. Wiescher, and D. G. Yakovlev (2005), “Nuclear fusion in dense matter: Reaction rate and carbon burning,” *Phys. Rev. C* **72**, 025806.
- Gebremariam, B, T. Duguet, and S. K. Bogner (2010), “Improved density matrix expansion for spin-unsaturated nuclei,” *Phys. Rev. C* **82**, 014305.
- Gentile, T R, and C. B. Crawford (2011), “Neutron charge radius and the neutron electric form factor,” *Phys. Rev. C* **83**, 055203.
- Gezerlis, Alexandros, and J. Carlson (2010), “Low-density neutron matter,” *Phys. Rev. C* **81** (2), 025803.
- Goriely, S, A. Bauswein, and H.-T. Janka, H.-T. (2011), “r-process nucleosynthesis in dynamically ejected matter of neutron star mergers,” *Astrophys. J. Lett.* **738**, L32.
- Goriely, S, and R. Capote (2014), “Uncertainties of mass extrapolations in Hartree-Fock-Bogoliubov mass models,” *Phys. Rev. C* **89** (5), 054318.
- Goriely, S, N. Chamel, and J. M. Pearson (2009), “Skyrme-Hartree-Fock-Bogoliubov nuclear mass formulas: Crossing the 0.6 mev accuracy threshold with microscopically deduced pairing,” *Phys. Rev. Lett.* **102**, 152503.
- Goriely, S, N. Chamel, and J. M. Pearson (2013), “Hartree-Fock-Bogoliubov nuclear mass model with 0.50 MeV accuracy based on standard forms of Skyrme and pairing functionals,” *Phys. Rev. C* **88**, 061302.
- Graham, Noah (2014), “Casimir energies of periodic dielectric gratings,” *Phys. Rev. A* **90**, 032507.
- Gusakov, ME, and P. Haensel (2005), “The entrainment matrix of a superfluid neutron–proton mixture at a finite temperature,” *Nucl. Phys. A* **761** (3–4), 333 – 348.
- Hanke, A, F. Schlesener, E. Eisenriegler, and S. Dietrich (1998), “Critical Casimir Forces between Spherical Particles in Fluids,” *Phys. Rev. Lett.* **81**, 1885–1888.
- Haxel, Otto, J. Hans D. Jensen, and Hans E. Suess (1949), “On the “magic numbers” in nuclear structure,” *Phys. Rev.* **75** (11), 1766–1766.
- de Heer, Walt A (1993), “The physics of simple metal clusters: experimental aspects and simple models,” *Rev. Mod. Phys.* **65** (3), 611–676.
- Hirsch, Jorge G, A. Frank, J. Barea, P. Van Isacker, and V. Velázquez (2005), “Bounds on the presence of quantum chaos in nuclear masses,” *Eur. J. Phys. A* **25** (1), 75–78.
- Hirsch, Jorge G, Víctor Velázquez, and Alejandro Frank (2004), “Quantum chaos and nuclear mass systematics,” *Phys. Lett. B* **595** (1–4), 231–236.
- Hohenberg, P, and W. Kohn (1964), “Inhomogeneous electron gas,” *Phys. Rev.* **136** (3B), B864–B871.
- Horowitz, C J, E. F. Brown, Y. Kim, W. G. Lynch, R. Michaels, A. Ono, J. Piekarewicz, M. B. Tsang, and H. H. Wolter (2014a), “A way forward in the study of the symmetry energy: Experiment, theory, and observation,” *J. Phys. G* **41**, 093001.
- Horowitz, CJ, K.S. Kumar, and R. Michaels (2014b), “Electroweak measurements of neutron densities in CREX and PREX at JLab, USA,” *Eur. Phys. J. A* **50** (2), 48, 10.1140/epja/i2014-14048-3.
- Jahn, H A, and E. Teller (1937), “Stability of polyatomic molecules in degenerate electronic states. I. orbital degeneracy,” *Proc. Roy. Soc. London* **161**, 220–236.
- Jones, R O, and O. Gunnarsson (1989), “The density functional formalism, its applications and prospects,” *Rev. Mod. Phys.* **61**, 689–746.
- Kac, Mark (1966), “Can one hear the shape of a drum?” *Am. Math. Monthly* **73** (4), 1–23.
- Klimchitskaya, G L, U. Mohideen, and V. M. Mostepanenko (2009), “The Casimir force between real materials: Experiment and theory,” *Rev. Mod. Phys.* **81**, 1827–1885.
- Kohn, W, and L. J. Sham (1965), “Self-consistent equations including exchange and correlation effects,” *Phys. Rev.* **140** (4A), A1133–A1138.
- Kortelainen, M, J. McDonnell, W. Nazarewicz, E. Olsen, P-G. Reinhard, J. Sarich, N. Schunck, S. M. Wild, D. Davesne, J. Erler, and A. Pastore (2014a), “Nuclear energy density optimization: Shell structure,” *Phys. Rev. C* **89**, 054314.
- Kortelainen, M, J. McDonnell, W. Nazarewicz, E. Olsen, P. G. Reinhard, J. Sarich, N. Schunck, S. M. Wild, D. Davesne, J. Erler, and A. Pastore (2014b), “Nuclear Energy Density Optimization: UNEDF2,” .

- Landau, LD (1956), “Theory of fermi liquids,” *Zh. Eksp. Teor. Fiz.* **30**, 1058–1064.
- Landau, LD (1957), “Oscillations of a Fermi liquid,” *Zh. Eksp. Teor. Fiz.* **32**, 59–66.
- Langake, K, and M. Wiescher (2001), “Nuclear reactions and stellar processes,” *Rep. Prog. Phys.* **64**, 1657–1701.
- Lattimer, James M (2014), “Symmetry energy in nuclei and neutron stars,” *Nucl. Phys.* **A928**, 276 – 295.
- Lesinski, T, T. Duguet, K. Bennaceur, and J. Meyer (2009), “Non-empirical pairing energy density functional,” *Eur. Phys. J. A* **40** (2), 121–126.
- Lipkin, H J (1958), “Center-of-mass motion in the nuclear shell model,” *Phys. Rev.* **110** (6), 1395–1397.
- Lunney, D, J. M. Pearson, and C. Thibault (2003), “Recent trends in the determination of nuclear masses,” *Rev. Mod. Phys.* **75** (3), 1021–1082.
- Magierski, P, and A. Bulgac (2004a), “Nuclear hydrodynamics in the inner crust of neutron stars,” *Acta Phys. Pol. B* **35** (3), 1203–1214.
- Magierski, P, A. Bulgac, and P.-H. Heenen (2003), “Exotic nuclear phases in the inner crust of neutron stars in the light of Skyrme-Hartree-Fock theory,” *Nucl. Phys. A* **719** (0), C217 – C220.
- Magierski, P, and P.-H. Heenen (2002a), “Structure of the inner crust of neutron stars: Crystal lattice or disordered phase?” *Phys. Rev. C* **65**, 045804.
- Magierski, Piotr, and Aurel Bulgac (2004b), “Nuclear structure and dynamics in the inner crust of neutron stars,” *Nucl. Phys. A* **738** (0), 143 – 149, proceedings of the 8th International Conference on Clustering Aspects of Nuclear Structure and Dynamics.
- Magierski, Piotr, and P.-H. Heenen (2002b), “Structure of the inner crust of neutron stars: Crystal lattice or disordered phase?” *Phys. Rev. C* **65**, 045804.
- Magierski, Piotr, Gabriel Wlazłowski, and Aurel Bulgac (2011), “Onset of a pseudogap regime in ultracold Fermi gases,” *Phys. Rev. Lett.* **107** (14), 145304.
- Magierski, Piotr, Gabriel Wlazłowski, Aurel Bulgac, and Joaquín E. Drut (2009), “Finite-temperature pairing gap of a unitary Fermi gas by quantum monte carlo calculations,” *Phys. Rev. Lett.* **103** (21), 210403.
- Mayer, Maria Goeppert (1949), “On closed shells in nuclei. ii,” *Phys. Rev.* **75** (12), 1969–1970.
- Mayer, Maria Goeppert (1950a), “Nuclear configurations in the spin-orbit coupling model. i. empirical evidence,” *Phys. Rev.* **78** (1), 16–21.
- Mayer, Maria Goeppert (1950b), “Nuclear configurations in the spin-orbit coupling model. ii. theoretical considerations,” *Phys. Rev.* **78** (1), 22–23.
- Meyer, B S (1989), “Decompression of initially cold neutron star matter - A mechanism for the r-process?” *Astrophys. J.* **343**, 254–276.
- Migdal, A B (1967), *Theory of Finite Fermi Systems and Applications to Atomic Nuclei* (Wiley, New York).
- Miller, GA, B.M.K. Nefkens, and I. Slaus (1990), “Charge symmetry, quarks and mesons,” *Phys. Rep.* **194**, 1–116.
- Miller, Gerald A, Allena K. Opper, and Edward J. Stephenson (2006), “Charge symmetry breaking and QCD,” *Annu. Rev. Nucl. Part. Sci.* **56**, 253–292.
- Molinari, A, and H. A. Weidenmüller (2006), “Nuclear masses, chaos, and the residual interaction,” *Phys. Lett. B* **637** (1–2), 48–52.
- Molinari, A, and H.A. Weidenmüller (2004), “Statistical fluctuations of ground-state energies and binding energies in nuclei,” *Phys. Lett. B* **601** (3–4), 119–124.
- Moller, P, J. R. Nix, W. D. Myers, and W. J. Swiatecki (1995), “Nuclear ground-state masses and deformations,” *At. Data. Nucl. Data Tables* **59** (2), 185–381.
- Möller, Peter, William D. Myers, Hiroyuki Sagawa, and Satoshi Yoshida (2012), “New finite-range droplet mass model and equation-of-state parameters,” *Phys. Rev. Lett.* **108**, 052501.
- Myers, W D, and W. J Swiatecki (1974), “The nuclear droplet model for arbitrary shapes,” *Ann. Phys. (NY)* **84** (1–2), 186–210.
- Myers, W D, and W. J Swiatecki (1990), “A thomas-fermi model of nuclei. part i. formulation and first results,” *Ann. Phys. (NY)* **204** (2), 401–431.
- Myers, W D, and W. J Swiatecki (1991), “A thomas-fermi model of nuclei. ii. fission barriers and charge distributions,” *Ann. Phys. (NY)* **211** (2), 292–315.
- Myers, W D, and W. J. Swiatecki (1996), “Nuclear properties according to the thomas-fermi model,” *Nucl. Phys. A* **601** (2), 141–167.
- Myers, William D, and W. J Swiatecki (1969), “Average nuclear properties,” *Ann. Phys. (NY)* **55** (3), 395–505.
- Myers, William D, and Wladyslaw J. Swiatecki (1966), “Nuclear masses and deformations,” *Nucl. Phys.* **81** (1), 1–60.
- Negele, J W (1970), “Structure of finite nuclei in the local-density approximation,” *Phys. Rev. C* **1** (4), 1260–1321.
- Negele, J W, and D. Vautherin (1972), “Density-matrix expansion for an effective nuclear hamiltonian,” *Phys. Rev. C* **5** (5), 1472–1493.
- Negele, J W, and D. Vautherin (1973), “Neutron star matter at sub-nuclear densities,” *Nucl. Phys. A* **207** (2), 298–320.
- Negele, J W, and D. Vautherin (1975), “Density-matrix expansion for an effective nuclear hamiltonian. ii,” *Phys. Rev. C* **11** (3), 1031–1041.
- Niksic, T, D. Vretenar, and P. Ring (2011), “Relativistic nuclear energy density functionals: Mean-field and beyond,” *Prog. Part. Nucl. Phys.* **66** (3), 519.
- Nishioka, H, Klavs Hansen, and B. R. Mottelson (1990), “Supershells in metal clusters,” *Phys. Rev. B* **42** (15), 9377–9386.
- Nolen, J A, and J P Schiffer (1969), “Coulomb Energies,” *Annu. Rev. Nucl. Sci.* **19** (1), 471–526.
- Oberacker, V E, and A. S. Umar (2015), “Density constrained TDHF,” arXiv:1502.04079.
- Olofsson, H, S. Åberg, O. Bohigas, and P. Leboeuf (2006), “Correlations in nuclear masses,” *Phys. Rev. Lett.* **96** (4), 042502.
- Olofsson, H, S. Åberg, and P. Leboeuf (2008), “Semiclassical theory of bardeen-cooper-schrieffer pairing-gap fluctuations,” *Phys. Rev. Lett.* **100** (3), 037005.
- Pedersen, J, S. Bjornholm, J. Borggreen, K. Hansen, T. P. Martin, and H. D. Rasmussen (1991), “Observation of quantum supershells in clusters of sodium atoms,” *Nature* **353** (6346), 733–735.
- Perdrisat, C F, V. Punjabi, and M. Vanderhaeghen (2007), “Nucleon electromagnetic form factors,” *Progress in Particle and Nuclear Physics* **59** (2), 694 – 764.
- Pizzochero, P M, L. Viverit, and R. A. Broglia (1997), “Vortex-nucleus interaction and pinning forces in neutron stars,” *Phys. Rev. Lett.* **79** (18), 3347 – 3350.
- Pizzochero, Pierre M (2007), “Pinning and Binding Energies for Vortices in Neutron Stars: Comments on Recent Results,”.
- Pizzochero, Pierre M (2011), “Angular Momentum Transfer in Vela-like Pulsar Glitches,”.
- Rahi, Sahand Jamal, Thorsten Emig, Noah Graham, Robert L. Jaffe, and Mehran Kardar (2009), “Scattering theory approach to electrodynamic Casimir forces,” *Phys. Rev. D* **80**, 085021.
- Reinhard, P-G, and W. Nazarewicz (2010), “Information content of a new observable: The case of the nuclear neutron skin,” *Phys. Rev. C* **81**, 051303.
- Ring, Peter, and Peter Schuck (2004), *The nuclear many-body problem*, 1st ed., Theoretical and Mathematical Physics Series No. 17 (Springer-Verlag, Berlin Heidelberg New York).
- Rosswog, S, O. Korobkin, A. Arcones, F.-K. Thielemann, and T. Piran (2014), “The long-term evolution of neutron star merger remnants



- I. The impact of r-process nucleosynthesis,” *MNRAS* **439**, 744–756.
- Schaden, Martin (2010), “Semiclassical estimates of electromagnetic Casimir self-energies of spherical and cylindrical metallic shells,” *Phys. Rev. A* **82**, 022113.
- Schram, S, and S. E. Koonin (1990), “Pycnonuclear fusion rates,” *Astrophys. J.* **365**, 296–300.
- Stetcu, I, C. Bertulani, A. Bulgac, P. Magierski, and K. J. Roche (2014), “Relativistic Coulomb excitation within Time Dependent Superfluid Local Density Approximation,” *Phys. Rev. Lett.* **114** (1), 012701.
- Stetcu, I, A. Bulgac, P. Magierski, and K. J. Roche (2011), “Isovector giant dipole resonance from the 3d time-dependent density functional theory for superfluid nuclei,” *Phys. Rev. C* **84**, 051309(R).
- Strutinsky, V M (1966), “Influence of nucleon shells on energy of a nucleus,” *Yad. Fiz.* **3** (4), 614–625, [*Sov. J. Nucl. Phys.* **3**, 449 (1966)].
- Strutinsky, V M (1967), “Shell effects in nuclear masses and deformation energies,” *Nucl. Phys. A* **95** (2), 420 – 442.
- Strutinsky, V M (1968), “‘Shells’ in deformed nuclei,” *Nucl. Phys. A* **122** (1), 1 – 33.
- Strutinsky, V M, and A. G. Magner (1976), “Semi-classical theory for nuclear shell structure,” *Fiz. Elem. Chastits At. Yadra* **7** (2), 356–478, [*Sov. J. Part. Nucl.* **7**, 138 (1976)].
- Tarbert, C M, D. P. Watts, D. I. Glazier, P. Aguar, J. Ahrens, J. R. M. Annand, H. J. Arends, R. Beck, V. Bekrenev, B. Boillat, A. Braghieri, D. Branford, W. J. Briscoe, J. Brudvik, S. Cherepnaya, R. Codling, E. J. Downie, K. Foehl, P. Grabmayr, R. Gregor, E. Heid, D. Hornidge, O. Jahn, V. L. Kashevarov, A. Knezevic, R. Kondratiev, M. Korolija, M. Kotulla, D. Krambrich, B. Krusche, M. Lang, V. Lisin, K. Livingston, S. Lugert, I. J. D. MacGregor, D. M. Manley, M. Martinez, J. C. McGeorge, D. Mekterovic, V. Metag, B. M. K. Nefkens, A. Nikolaev, R. Novotny, R. O. Owens, P. Pedroni, A. Polonski, S. N. Prakhov, J. W. Price, G. Rosner, M. Rost, T. Rostomyan, S. Schadmand, S. Schumann, D. Sober, A. Starostin, I. Supek, A. Thomas, M. Unverzagt, Th. Walcher, L. Zana, and F. Zehr (2014), “Neutron Skin of 208Pb from Coherent Pion Photoproduction,” *Phys. Rev. Lett.* **112**, 242502.
- Tondeur, F (1978), “An energy density nuclear mass formula: (i). self-consistent calculation for spherical nuclei,” *Nucl. Phys. A* **303** (1–2), 185 – 198.
- Umar, A S, and V. E. Oberacker (2006), “Heavy-ion interaction potential deduced from density-constrained time-dependent Hartree-Fock calculation,” *Phys. Rev. C* **74**, 021601.
- Umar, A S, V. E. Oberacker, C. J. Horowitz, P.G. Reinhard, and J. A. Maruhn (2015), “Swelling of nuclei embedded in neutron-gas and consequences for fusion,” arXiv:1505.03189.
- Vardanyan, GA, and D. M. Sedrakyan (1981), “Magnetohydrodynamics of superfluid solutions,” *Sov. Phys.–JETP* **81**, 1731–1737.
- Viñas, X, M. Centelles, X. Roca-Maza, and M. Warda (2014), “Density dependence of the symmetry energy from neutron skin thickness in finite nuclei,” *Eur. Phys. J. A* **50** (2), 27.
- Volovik, G E, V. P. Mineev, and I. M. Khalatnikov (1975), “Theory of solutions of a superfluid Fermi liquid in a superfluid Bose liquid,” *Zh. Eksp. Teor. Fiz.* **42** (2), 342–347.
- Waechter, R T (1972), “On hearing the shape of a drum: an extension to higher dimensions,” *Math. Proc. Cambridge Philos. Soc.* **72** (3), 439–447.
- Wang, M, G. Audi, A.H. Wapstra, F.G. Kondev, M. MacCormick, X. Xu, and B. Pfeiffer (2012), “The ame2012 atomic mass evaluation,” *Chinese Phys. C* **36** (12), 1603.
- Weizsäcker, C F v (1935), “Zur theorie der kernmassen,” *Z. Phys. A* **96**, 431–458.
- Weyl, H (1911), “Über die asymptotische verteilung der eigenwerte,” *Nachr. Königl. Ges. Wiss. Göttingen*, 110–117.
- Weyl, Hermann (1912a), “Das asymptotische verteilungsgesetz der eigenwerte linearer partieller differentialgleichungen (mit einer anwendung auf die theorie der hohlraumstrahlung),” *Math. Ann.* **71** (4), 441–479.
- Weyl, Hermann (1912b), “Über das spektrum der hohlraumstrahlung,” *J. f. d. reine u. angew. Math.* **141**, 163.
- Weyl, Hermann (1912c), “Über die abhängigkeit der eigenschwingungen einer membran und deren begrenzung,” *J. f. d. reine u. angew. Math.* **141**, 1.
- Weyl, Hermann (1913), “Über die randwertaufgabe der strahlungstheorie und asymptotische spektralgesetze,” *J. f. d. reine u. angew. Math.* **143**, 177.
- Weyl, Hermann (1915), “Das asymptotische verteilungsgesetz der eigenschwingungen eines beliebig gestalteten elastischen körpers,” *Rend. Circ. Mat. Palermo* **39** (1), 1–49.
- Weyl, Hermann (1950), “Ramifications, old and new, of the eigenvalue problem,” *Bull. Amer. Math. Soc.* **56** (2), 115–139.
- Wlazłowski, G, J. W. Holt, S. Moroz, A. Bulgac, and K. J. Roche (2014), “Auxiliary-field quantum Monte Carlo simulations of neutron matter in chiral effective field theory,” *Phys. Rev. Lett.* **113**, 182503.
- Wlazłowski, Gabriel, Aurel Bulgac, Michael McNeil Forbes, and Kenneth J. Roche (2015), “Life cycle of superfluid vortices and quantum turbulence in the unitary Fermi gas,” *Phys. Rev. A* **91**, 031602.
- Wlazłowski, Gabriel, and Piotr Magierski (2010), “Superfluid properties of dilute neutron matter,” *Int. J. Mod. Phys. E* **20**, 569–575.
- Wlazłowski, Gabriel, and Piotr Magierski (2011), “Quantum Monte Carlo study of dilute neutron matter at finite temperatures,” *Phys. Rev. C* **83** (1), 012801.
- Yu, Yongle, and Aurel Bulgac (2003a), “Energy density functional approach to superfluid nuclei,” *Phys. Rev. Lett.* **90**, 222501.
- Yu, Yongle, and Aurel Bulgac (2003b), “Spatial structure of a vortex in low density neutron matter,” *Phys. Rev. Lett.* **90**, 161101.
- Yu, Yongle, and Aurel Bulgac (2003c), “Spatial structure of a vortex in low density neutron matter,” *Phys. Rev. Lett.* **90**, 161101.
- Yu, Yongle, Aurel Bulgac, and Piotr Magierski (2000), “Shell Correction Energy for Bubble Nuclei,” *Phys. Rev. Lett.* **84**, 412–415.
- Zwinger, Wilhelm, Ed. (2012), *The BCS–BEC Crossover and the Unitary Fermi Gas*, Lecture Notes in Physics, Vol. 836 (Springer-Verlag, Berlin Heidelberg).